The Development and Neurophysiological Assessment of Newborn Auditory Cognition: A Review of Findings and Their Application

Josef Urbanec[1,2,*], Jan Kremláček[1,3], Kateřina Chládková[4,5], Sylva Skálová[6]

ABSTRACT

This review article introduces the basic principles of infants' neurophysiology, while summarizing the core knowledge of the anatomical structure of the auditory pathway, and presents previous findings on newborns' neural speech processing and suggests their possible applications for clinical practice. In order to tap into the functioning of the auditory pathway in newborns, recent approaches have employed electrophysiological techniques that measure electrical activity of the brain. The neural processing of an incoming auditory stimulus is objectively reflected by means of auditory event-related potentials. The newborn's nervous system processes the incoming sound, and the associated electrical activity of the brain is measured and extracted as components characterized by amplitude, latency, and polarity. Based on the parameters of event-related potentials, it is possible to assess the maturity of a child's brain, or to identify a pathology that needs to be treated or mitigated. For instance, in children with a cochlear implant, auditory event-related potentials are employed to evaluate an outcome of the implantation procedure and to monitor the development of hearing. Event-related potentials turn out to be an irreplaceable part of neurodevelopmental care for high-risk children e.g., preterm babies, children with learning disabilities, autism and many other risk factors.

KEYWORDS

newborns; auditory pathway; cortical auditory evoked potentials; maturation of the central nervous system; learning disabilities

AUTHOR AFFILIATIONS

[1] Department of Pathological Physiology, Medical Faculty in Hradec Králové, Charles University, Czech Republic
[2] Paediatrics Department, Havlíčkův Brod Hospital, Czech Republic
[3] Department of Medical Biophysics, Medical Faculty in Hradec Králové, Charles University, Czech Republic
[4] Institute of Psychology, Czech Academy of Sciences, Prague, Czech Republic
[5] Institute of Czech Language and Theory of Communication, Faculty of Arts, Charles University, Prague, Czech Republic
[6] Paediatrics Department of University Hospital in Hradec Králové, Charles University, Czech Republic
* Corresponding author: Department of Pathological Physiology, Medical Faculty in Hradec Králové, Charles University, Czech Republic; e-mail: jurbanec86@gmail.com

Received: 9 February 2021
Accepted: 14 January 2022
Published online: 29 June 2022

Acta Medica (Hradec Králové) 2022; 65(1): 1–7
https://doi.org/10.14712/18059694.2022.9

INTRODUCTION

The neonatal period is defined as the interval from birth to the 28th day of an infant's life. Despite being marked by its beginning and end points, the neonatal period should – in many respects – be understood as a direct continuation of intrauterine development. According to knowledge of auditory perception, it is well-established that the fetus can hear and process surrounding stimuli and adequate prenatal auditory stimulation is necessary for normal development of hearing (1, 2).

After birth, hearing becomes one of the fundamental senses that stimulate the early development of a child's cognitive functions, thus contributing to the acquisition of speech, language, and abstract thinking. Intact peripheral and central part of the auditory apparatus is necessary for a child's psychomotor development. As hearing impairment may interfere with cognitive and psychomotor development, it is crucial to detect this deficit as soon as possible. Subsequent intervention, e.g. with a cochlear implant (CI), may reduce impact on all aspects of later life quality (3–7). For this reason, objective screening methods focused on auditory perception are typically performed. The most common is the assessment of transient evoked otoacoustic emissions (TEOAE). This approach can assess the functionality of cochlea (the peripheral part of the auditory apparatus) but cannot measure whether the information has also been correctly processed by the

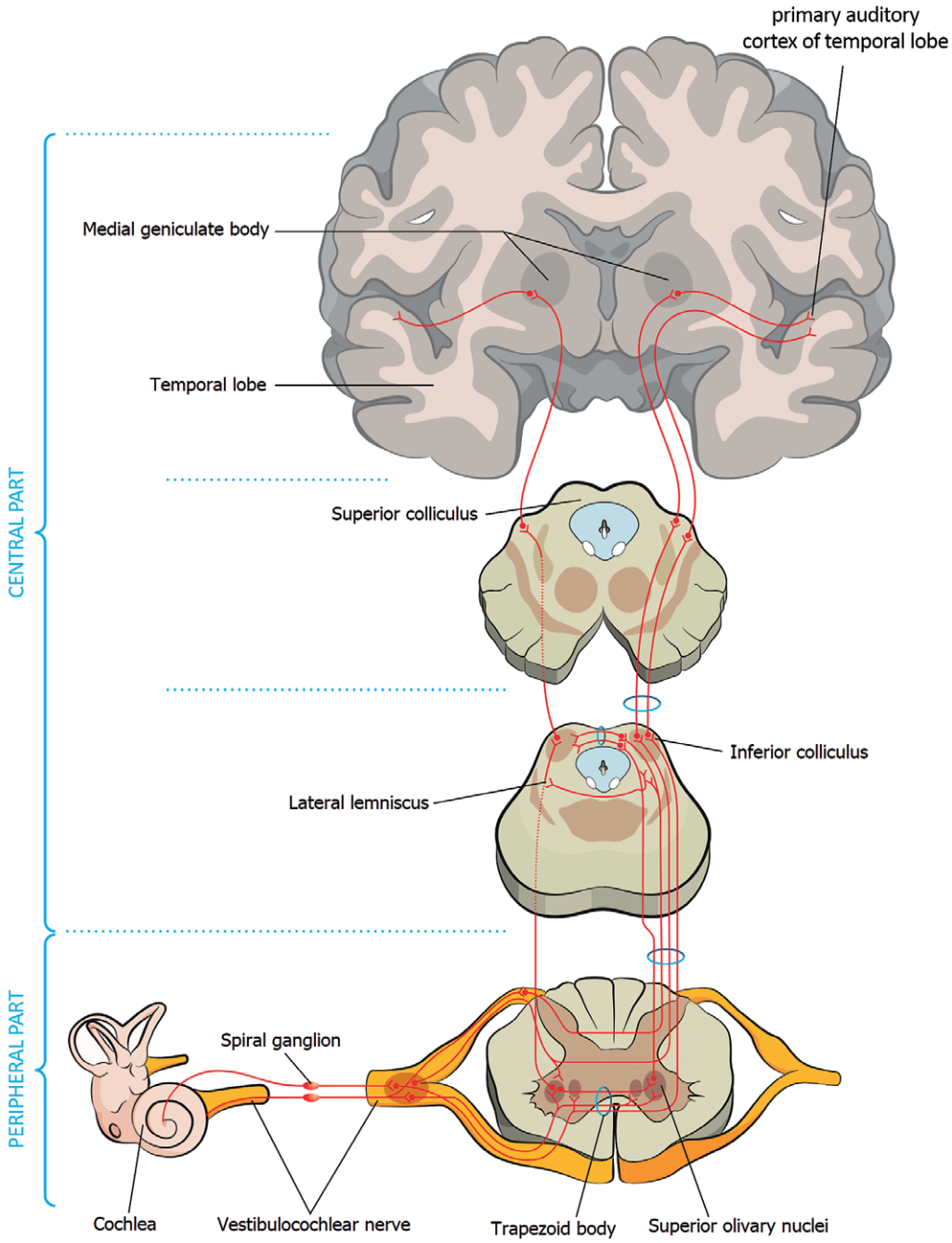

Fig. 1 Anatomical structure of the auditory pathway can be divided into a peripheral part, including the cochlea as a sensory organ, and a central part that conducts electrical potentials through the brain stem and midbrain to the primary cortical region, where it is subsequently evaluated and processed (scheme adopted and freely modified according to (1)).

central nervous system (CNS). Improper engagement and functioning of the higher auditory areas can lead to disorders such as the auditory processing deficit, dyslexia, or learning disability (3, 8). Detection of the brainstem, early, and later evoked potentials, also called event-related potentials (ERPs), allow us to examine the subsequent stages of auditory stimulus processing. These techniques objectively test the functional integrity of the auditory system by measuring the brain's response to auditory stimuli (9).

ANATOMY OF AUDITORY PATHWAY

The auditory pathway is distinguished into the peripheral and the central part, also called structural and neurosensorial, respectively (Figure 1). These two parts differ not only in their function, but also in the timeline of their development. The peripheral part consists of the outer, middle, and inner ear. It participates in capturing and converting an incoming auditory stimulus (mechanical sound waves) into electrical potential, which is transferred to the central auditory system (1). The division of the peripheral system into the outer, middle, and inner ear mostly follows the development of primary germ layers or their derivatives (Figure 2A–D). The base of the inner ear forms at the beginning of the fourth gestational week and its development completes in the 20th gestational week (1, 10, 11).

It is through the vestibulocochlear nerve that the auditory receptor potential reaches the brainstem, afterwards switching to the mesencephalon, thalamus, and finally the cerebral cortex. The primary auditory cortex is in the temporal lobe, in the tonotopically arranged area 41 (Figure 1). The axons end in the associative cortical regions areas 42 and 22. This part of the auditory system does not develop fully until the 20th gestational week (12, 13).

The cochlea of the inner ear and the auditory cortical networks in the temporal lobe are, developmentally, the most sensitive clinical components of the auditory pathway. They may be affected during intrauterine

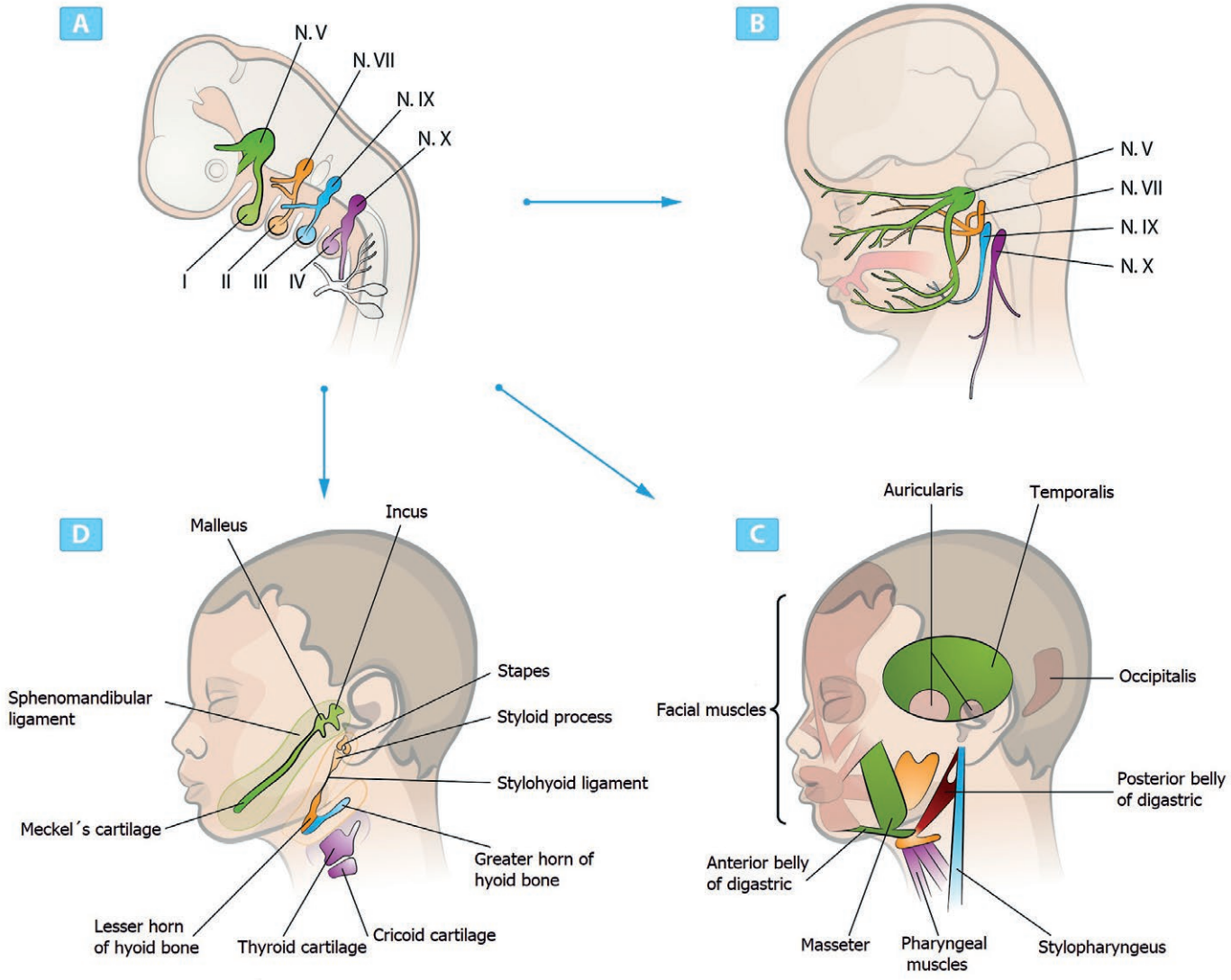

Fig. 2A–D Diagram of the gill arches and their development (marked with Roman numerals I-IV, color distribution respects the origin of tissues from individual arches also in the following figures B–D). Figures A and B also show the origin of cranial nerves important for innervation in the facial region (labeled N.V-N.X). The gill arches I and II give rise to the transmission system of the middle ear, the peripheral part of the auditory pathway. Gill arch I also develops into the tensor tympani muscle, which participates in the transmission of sound by changing the drum voltage (scheme adopted and freely modified according to (11)).

development, e.g. by prenatal infection, but also in the neonatal period due to antibiotic treatment, or exposure to noise in a neonatal intensive care unit (14). This vulnerability stems largely from the gradual maturation of the sensitive neurosensory part (the hair cells of the inner ear), axons and neurons, that takes place between the 25th gestational week and the fifth month of life (1).

The auditory pathway can transmit the surrounding sound stimuli to the developing fetal brain already between the 25th and the 29th gestational week. During gestation, the uterus is a natural barrier protecting the fetus from intensive impacts that could harm its development, limiting the intensity as well as the spectral content of the incoming sound (1, 3, 15). However, even in the rather attenuated and somewhat distorted sound, a physiologically developing fetus can recognize various frequently encountered sounds, most notably the rhythm and melody of its mother's speech (16). Prenatal auditory stimulation aids the development of the tonotopic organization of the cochlear hair cells and the auditory cortex (14). After birth, when the attenuating barrier disappears, the incoming auditory stimuli contribute to further cortical development. From the perspective of hearing, the neonatal period is an uninterrupted continuation of intrauterine development (1, 2). This is evidenced by a study that compared the development of hearing with vision. While vision develops only after birth, auditory stimulation with varied naturalistic stimuli (e.g. maternal voice, music, or common environmental sounds) during the last 10–12 weeks of the fetal period *in utero* or in prematurely born infants seems to be essential for proper hearing development (1).

CORTICAL EVOKED POTENTIALS

Neuronal activity induced by auditory stimulation can be detected as evoked potentials, at many different levels of the auditory pathway. The measurement of evoked potentials is a non-invasive, dynamic, and objective method based on the principle of electroencephalography (EEG) sensing the electrical activity of the brain. Cortical Auditory Evoked Potentials (CAEPs) are often measured to assess auditory perception. They belong to a broader group of ERPs, sometimes called cognitive ERPs (9). ERPs extraction is done by averaging epochs of the EEG that are aligned to the occurrence of repeatedly presented acoustic stimuli (12, 17).

To assess the trajectory of auditory processing one typically evaluates the components, i.e. the peaks and their latencies, within the averaged ERPs. The advantage of the ERP method is its fine temporal resolution, which allows to accurately measure the peak time of a response, i.e., the latency, in milliseconds (9). The strongest CAEPs can be recorded in the back of lateral sulcus, the so-called Sylvian fissure, which separates the frontal and temporal lobes. Due to the non-invasive character of EEG recording the exact localization of CAEPs is not possible (12, 17).

With some simplification, CAEPs can be divided into exogenous (sometimes inaccurately called *obligatory*) and endogenous (inaccurately called *cognitive*) components. Exogenous components reflect the physical properties of the sound, such as the intensity, frequency, and duration, whereas endogenous components are modulated by neuronal activity in higher cortical centres and are not determined solely by the sound's physical properties (17).

Exogenous components include the P50, N100, P200, and N200. In newborns, unlike in older children, P100 and N100 waves are not well detectable. Newborns' ERPs typically have a relatively broad peak at 200–300 ms latency, called P200, which is followed by a broad negative N200 wave at 300–600 ms latency. The latencies and breadth of the P200 and N200 waves decrease markedly in the course of the first months after birth (9, 12).

Endogenous components are used to evaluate higher-level, e.g. linguistic, processing of auditory stimuli by the newborn brain. These components include the *mismatch response* (MMR) (18), P300, and N400. MMR, one of the most frequently evaluated components, is defined as a difference in the potential induced by a rarely occurring, i.e. *deviant,* stimulus, and the potential induced by a frequently repeated, i.e. *standard,* stimulus (Figure 3). The MMR is roughly interpretable as an index of prediction error originating from a comparison of a novel unexpected deviant stimulus against a built-up memory trace for the previously presented frequent standard stimuli (12). The MMR component is elicited automatically and does not require conscious attention to the stimuli, and can be also measured during (active) sleep. If a deviant sound is perceived as different from previously presented standard sounds, it elicits the MMR, typically at a latency of 100–250 ms relative to the onset of the deviation. The larger the perceived difference between the deviant and the standard stimulus, the larger the MMR amplitude and/or the shorter its latency. In adults, the MMR is typically bilateral in both temporal and frontal cortical areas (12) and has a negative polarity (hence in adults it is referred to as *mismatch negativity*, MMN, see Figure 3). In infants, however, MMR often has a positive polarity (3), indicating imperfect maturation and/or marginal audibility of the acoustic difference between the deviant and the standard stimulus (4).

Besides the age-related differential polarity, the MMR latency is in newborns greater than in adults and decreases gradually mainly during the first two years of life. Ontogenetically, the MMR is a very early potential detectable from the 30th postconceptional week (14, 17). Newborns' MMR, similarly to adults' MMN, reflects rather fine phonetic discrimination abilities, such as the ability to distinguish sounds coming from different sources, or the ability to detect both a change in speaker voice and in speech sound quality (9). This observation in healthy newborns indicates that the neonatal brain has a fully developed discriminatory capacity for sound stimuli (17), although its CNS structures are not yet fully mature (19–21). Newborns' MMR also indexes the ability to differentiate variations in auditory stimuli that are important for speech and language development (17). In child auditory perception, developmental speech disorders or learning difficulties are often associated with an attenuated or delayed MMR response (3). MMR is therefore well suited to assess the earliest stages of cognitive development, particularly the speech and language capacity of the developing individual.

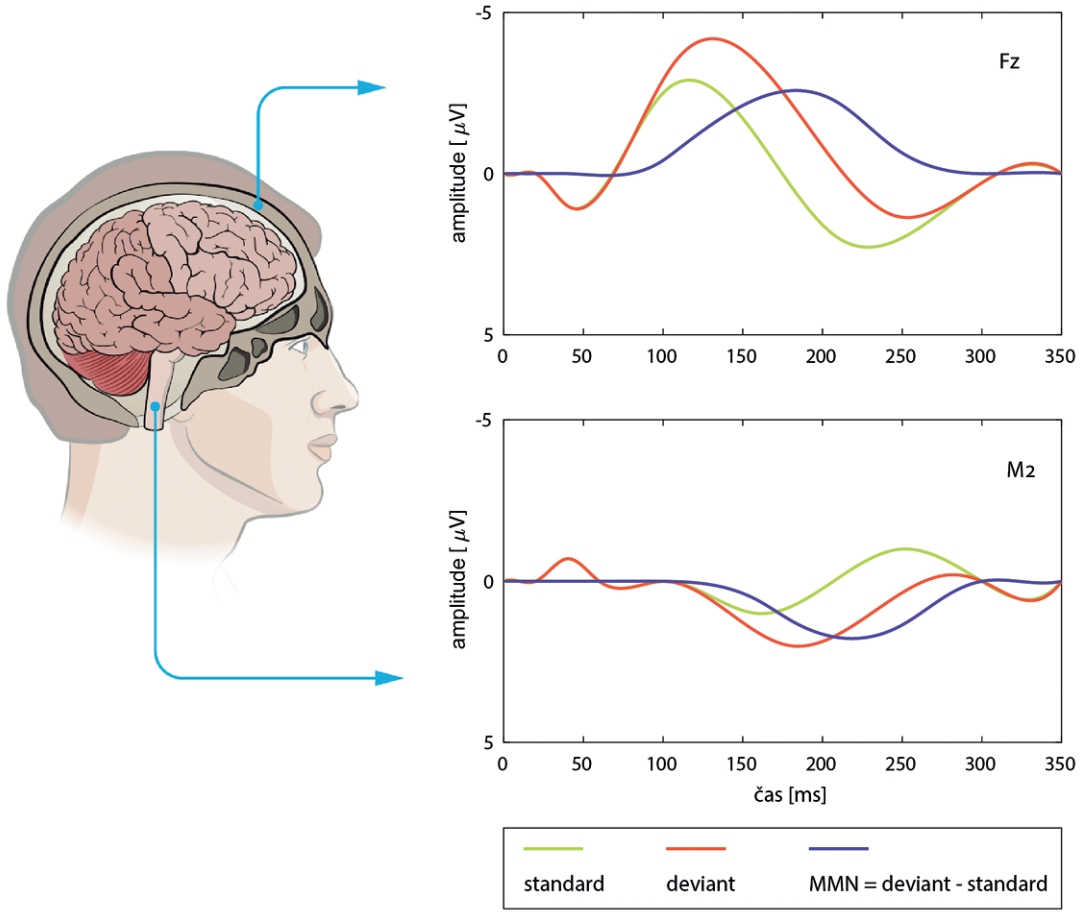

Fig. 3 Schematic representation of cortical auditory evoked potentials (CAEP) sensed by an electrode placed above the frontal area (Fz) and the processus mastoideus (M2). The frequent, standard stimulus is represented by a green curve, the rare, deviant stimulus by an orange curve. The subsequent amplitude difference of both stimuli is highlighted by a blue curve as the so-called difference wave, which peaks as mismatch negativity (MMN) at latency of about 200 ms. The amplitude of the MMN tends to be positive when measured with an electrode above the mastoid processus, in other locations it typically, in adults, has negative values (scheme adopted and freely adjusted according to (17)).

STUDIES WITH NEWBORNS

Several studies have assessed and evaluated auditory cognitive potentials in neonates. Most of studies test healthy newborns and apply inclusion criteria such as the absence of neurological disorders, medication, pre- or peripartal complications, excessive physical activity during the assessment, and need a passed neonatal hearing screening – brainstem auditory evoked potentials, steady state response auditors or TEOAE (4, 19). In previous studies, healthy newborns meeting the above criteria are typically compared to e.g. preterm newborns, infants with suspicion of hearing impairment, deficient neural speech processing, or high familial risk for a developmental language or speech disorder.

Melo et al. (2016) compared the cognitive evoked potentials of 31 preterm and 66 term infants. The infants were tested in sleep, after feeding, using biaural auditory stimulation. The syllable /ba/ served as the frequent standard stimulus, and /ra/ served as the rare deviant stimulus. The P100 and N100 waves were less likely to be present in preterm as compared to full term infants (they were missing in 13% and 4.5% of cases, respectively). No significant differences in the incidence of N200 or P200 were found between the two groups. The absence of the P100 wave in CAEP in premature infants can be a possible indicator of cognitive delays or immature cortical structures in this population. Besides evaluating the absence/presence of P100 (and N100), the latency of ERPs components can, be used too as an indicator of immaturity inversely proportional to gestational age (4).

The results of that study are in line with the results of other studies comparing the maturation of the infant brain. Exogenous components have longer latency in newborns than in older children, and the latency rapidly decreases in the first and second year of life. This may be caused by the development of synapses during the first years of life, reflected in an increase of low-frequency EEG activity, which is also the frequency range relevant for the ERPs. Continuing myelination at pre-school age leads to more adult-like ERPs.

In general, ERP latency thus mostly reflects the maturation of the CNS itself. ERP amplitude, on the contrary, seems to correlate with the number of neural structures involved in the response (number of synapses). Early developmental changes in the amplitude of the auditory ERP

thus seem to depend mainly on gestational age, and less so on the amount of (extrauterine) auditory exposure (2, 4, 20, 21).

A recent study by Oliveira et al. (2019) assessed CAEPs in 39 full-term newborns (19). The measurements were monoaural with a randomly selected ear stimulated by pure tones of various frequencies. At an initial sound intensity of 80 dB SPL, latency and amplitude did not show statistically significant differences for various stimulus frequencies. However, the latency of the P100 wave was inversely proportional to stimulus intensity. One of the conclusions of this study was that compared to the brain stem response, the cortical auditory ERPs are elicited only if stimulus intensity exceeds a particular threshold (2, 19). The fact that the brain stem response is elicited also at a lower stimulus intensity can be attributed to a faster maturation of the subcortical, compared to cortical centres. Some other studies found that the latencies of P100 and N100 are greater for pure tones than for speech stimuli (19, 22).

ERPs can be used not only to assess CNS maturation, but also to quantify the success of intervention in children with hearing disorders, especially with deafness. Silva et al. (2014) have shown that auditory cognitive potentials can verify the level of auditory stimulation needed for the maturation of the CNS in children with CI. For instance, there seems to be a relationship between the P100 wave, measured immediately after CI implantation, and the onset of vocalisation in children with different ages of CI implantation (6). After implantation, which positively affects the child's communicative development, one can objectively assess changes in the CNS, namely, a decrease of the P100 latency to tones and speech stimuli (4–7).

The CAEPs may assess the effect of CI implantation and normalization of auditory development but could also detect deafness in children. Mehta et al. (2017) described the role of the CAEPs for early diagnosis and later therapy in children with hearing loss in United Kingdom during 2011–2015. That study compared 2 sequential cohorts of children with a permanent childhood hearing impairment and with different time of CI implantation. The first cohort included 34 children examined prior the introduction of CAEPs, the second 44 children examined after the introduction of CAEPs. The only difference in the patient pathway was the use of CAEPs in diagnosis and therapy. Except the common examination, for the second infants group diagnosis included CAEPs to speech tokens /m/ (duration of 30 ms), /g/ (duration 20 ms), and /t/ (duration of 30 ms) presented at nominal intensity 55, 65 and 75 dB SPL. Early hearing aid fitting was recommended if the response for /g/ or /t/ at 55 dB SPL was missing. Additionally, a second CAEPs session 4 to 8 weeks later was performed for all children without a recommendation of early hearing aid at the first session. If the CAEPs (at second session) were absent at 75 dB SPL in infants optimally fitted with hearing aids, referral for CI assessment was recommended. The results showed that children with severe deafness were referred significantly earlier for CI assessment after the introduction of CAEPs than before: the median age of hearing aid fitting for children with all degrees of hearing impairment decreased from 9.2 months to 3.9 months after the introduction of CAEPs examination. This trend was observed also in children with mild or moderate hearing loss (median age decreased from 19 to 5 months) (7).

There are other areas in which CAEPs seem promising as an early diagnostic tool for developmental disorders. Thiede et al. (2019) performed a longitudinal study with 44 newborns at high familial risk of dyslexia and with a control group of 44 low-risk newborns. The newborns were stimulated by pseudowords with changes from a standard /tata/ stimulus in vowel duration /tata:/, vowel spectrum /tato/ and pitch /ta^{ta}/ at stimulus intensity 65 dB SPL. EEG recordings were analysed for MMR to each type of change. The results suggested atypical neural discrimination of speech sound differences in the high-risk newborns: their MMR were diminished or completely absent, had longer latency and different hemispheric lateralization and morphology compared to infants with no dyslexia in family history (3).

CONCLUSIONS AND CLINICAL APPLICATION

The auditory pathway is a necessary and irreplaceable connection of the developing fetus with the outside world. The peripheral and central auditory system development starts already in the prenatal period and at birth, hearing seems comparable in pre-term and term neonates (4). At the 40th gestational week, auditory cognitive potentials of premature and term-born infants do not seem to differ significantly, indicating that extrauterine stimulation does not alter the maturation of auditory processes in the pre- and postnatal period (17). Auditory ERPs display maturational changes throughout infants' development. Throughout infancy there is a clear developmental decrease in latency which is comparable across children born premature and children born full-term (same gestational age), despite the former group having had longer exposure to sounds *ex utero*, which aligns well with the gradual maturation of CNS structures across the intrauterine and extrauterine periods of development (19, 21).

The absence or reduced amplitude of ERP components can be used for diagnosis and evaluation of pathologies. As an example, MMR deficiency is often associated with learning disorders, cleft palate, autism or Asperger syndrome, depression or behavioural disorders. In children with very low birth weight and speech impairment, reduced MMR amplitude was found at four to six years of age (9). This reduction in MMR amplitude is to be associated with speech impairment rather than with the child's maturation at birth because, as noted above, the amplitude and latency of the measured cognitive potential components are comparable between term and very-low-birth-weight (premature) children (4, 17).

To conclude, electrophysiological methods are routinely employed to monitor neonatal hearing but here we show that they could have a greater application in the clinical practice as they can help assess the very development and maturation of the newborns' auditory pathway. Maturation of CNS depends primarily on the myelination of nerve fibers, which lead the signal to the corresponding

cortical centres which generate the cortical evoked potentials (19). Moreover, early and developmental evaluation of auditory ERPs is a promising approach that may find application in monitoring the dynamics of some developmental disorders and diseases such as dyslexia, autism (3, 8, 14). Based on recent findings which were reviewed in this article, we suggest that CAEPs should become an integral part of clinical practice to evaluate children's auditory development.

DEDICATION

Supported by the projects of Charles University PRIMUS/17/HUM/19 a PROGRES Q40/07.

REFERENCES

1. Graven S, Browne J. Auditory Development in the Fetus and Infant. NbInfant Nurs Rev 2008; 8(4): 187–93.
2. Sousa A, Didoné D, Sleifer P. Longitudinal Comparison of Auditory Steady-State Evoked Potentials in Preterm and Term Infants: The Maturation Process. Int Arch Otorhinolaryngol 2017; 21(3): 200–5.
3. Thiede A, Virtala P, Ala-Kurikka I, et al. An extensive pattern of atypical neural speech-sound discrimination in newborns at risk of dyslexia. Clin Neurophysiol 2019; 130(5): 634–46.
4. Melo de A, Biaggio E, Rechia I, et al. Cortical auditory evoked potentials in full-term and preterm neonates. Codas 2016; 28(5): 491–6.
5. Martins K, Gil D. Cortical Auditory Evoked Potentials with Simple (Tone Burst) and Complex (Speech) Stimuli in Children with Cochlear Implant. Int Arc Otorhinolaryngol 2017; 21(4): 351–7.
6. Silva L, Couto M, Tsuji R, et al. Auditory pathways' maturation after cochlear implant via cortical auditory evoked potentials. Braz J Otorhinolaryngol 2014; 80(2): 131–7.
7. Mehta K, Watkin P, BAldwin M, et al. Role of Cortical Auditory Evoked Potentials in Reducing the Age at Hearing Aid Fitting in Children With Hearing Loss Identified by Newborn Hearing Screening. Trends in Hearing 2017; 21.
8. Frizzo, A. Auditory evoked potential: a proposal for further evaluation in children with learning disabilities. Front Psychol 2015; 6: 788.
9. Duncan C, Barry R, Connolly J, et al. Event-related potentials in clinical research: Guidelines for eliciting, recording, and quantifying mismatch negativity, P300, and N400. Clin Neurophysiol 2009; 120(11): 1883–908.
10. Vacek Z. Organogeneze. Embryologie: učebnice pro studenty lékařství a oborů všeobecná sestra a porodní asistentka. Praha: Grada 2006: 99–101, 235–8.
11. Carlson, M. Nervous system. In: Human embryology and developmental biology, 5th ed. Philadelphia, PA: Elsevier/Saunders 2014: 216–45.
12. Joos K, Gilles A, Van de Heyning P, et al. From sensation to percept: The neural signature of auditory event-related potentials. Neurosci Biobehav R 2014; 42: 148–56.
13. Druga R, Grim M, Dubový P. Přehled drah CNS. Anatomie CNS. Praha: Galén 2011: 208–10.
14. Lahav A, Skoe E. An acoustic gap between the NICU and womb: a potential risk for compromised neuroplasticity of the auditory system in preterm infants. Front Neurosci 2014; 8: 381.
15. Wodicka G, M. Lam A, Bhargava V, et al. Acoustic impedance of the maternal abdomen. J Acoust Soc Am 1993; 94(1): 13–18.
16. Granier-Deferre C, Ribeiro A, Jacquet AY, et al. Near-term fetuses process temporal features of speech. Dev Sci 2011; 14(2): 336–52.
17. Fellman V, Huotilainen M. Cortical auditory event-related potentials in newborn infants. Semin Fetal Neonatal Med 2006; 11(6): 452–8.
18. Naatanen R, Picton T. The N1 wave of the human electric and magnetic response to sound: a review and an analysis of the component structure. Psychophysiology 1987; 24(4): 375–425.
19. Oliveira L, Didoné D, Durante A. Automated cortical auditory evoked potentials threshold estimation in neonates. Braz J Otorhinolaryngol 2019; 85(2): 206–12.
20. Portonova G, Martynova O, Ivanitsky G. Age differences of event-related potentials in the perception of successive and spatial components of auditory information. Hum Physiol 2014; 40(1): 20–8.
21. Pena M, Werker J, Dehaene-Lambertz G. Earlier Speech Exposure Does Not Accelerate Speech Acquisition. J Neurosci 2012; 32(33): 11159–63.
22. Cone B, Whitaker R. Dynamics of infant cortical auditory evoked potentials (CAEPs) for tone and speech tokens. Int J Pediatr Otorhinolaryngol 2013; 77(7): 1162–73.

Dose-Dependency of Toxic Signs and Outcomes of Paraoxon Poisoning in Rats

Žana M. Maksimović[1,*], Ranko Škrbić[1,2], Miloš P. Stojiljković[1,2]

ABSTRACT

Organophosphorus compounds induce irreversible inhibition of acetylcholinesterase, which then produces clinically manifested muscarinic, nicotinic and central effects. The aim of the study was to analyse the clinical signs of acute paraoxon poisoning in rats and to determine the relationship between the intensity of signs of poisoning and the dose of paraoxon and/or the outcome of poisoning in rats. Animals were treated with either saline or atropine (10 mg/kg intramuscularly). The median subcutaneous lethal dose (LD_{50}) of paraoxon was 0.33 mg/kg and protective ratio of atropine was 2.73. The presence and intensity of signs of poisoning in rats (dyspnoea, lacrimation, exophthalmos, fasciculations, tremor, ataxia, seizures, piloerection, stereotypic movements) were observed and recorded for 4 h after the injection of paraoxon. Intensity of these toxic phenomena was evaluated as: 0 – absent, 1 – mild/moderate, 2 – severe. Fasciculations, seizures and tremor were more intense at higher doses of paraoxon and in non-survivors. In unprotected rats piloerection occurred more often and was more intense at higher doses of paraoxon as well as in non-survivors. In atropine-protected rats, piloerection did not correlate with paraoxon dose or outcome of poisoning. The intensity of fasciculations and seizures were very strong prognostic parameters of the poisoning severity.

KEYWORDS

organophosphate; insecticide; paraoxon; poisoning; acetylcholinesterase inhibitor; atropine

AUTHOR AFFILIATIONS

[1] Centre for Biomedical Research, Faculty of Medicine, University of Banja Luka, Banja Luka, the Republic of Srpska, Bosnia and Herzegovina
[2] Department of Pharmacology, Toxicology and Clinical Pharmacology, Faculty of Medicine, University of Banja Luka, Banja Luka, the Republic of Srpska, Bosnia and Herzegovina
* Corresponding author: Centre for Biomedical Research, Faculty of Medicine, University of Banja Luka, Banja Luka, the Republic of Srpska, Bosnia and Herzegovina; e-mail: zana.maksimovic@med.unibl.org

Received: 9 July 2021
Accepted: 23 February 2022
Published online: 29 June 2022

Acta Medica (Hradec Králové) 2022; 65(1): 8–17
https://doi.org/10.14712/18059694.2022.10

INTRODUCTION

Acetylcholinesterase (AChE, EC 3.1.1.7) is a very potent enzyme whose role is to break down acetylcholine (ACh) in the synaptic cleft (1, 2). Inhibition of AChE results in the accumulation of ACh and excessive stimulation of cholinergic receptors. AChE inhibitors (AChEI) can be reversible (carbamate compounds) and irreversible (organophosphorus compounds – OPCs) (3–5). OPCs form a stable covalent bond with AChE, which is not spontaneously hydrolysed (6). They are divided into two major groups, nerve agents (tabun, sarin, soman, VX) (7) and organophosphorus insecticides (OPI). Paraoxon (diethyl (4-nitrophenyl) phosphate) is an active metabolite of the highly toxic OPI parathion (8). Among the OPIs, paraoxon is very similar to nerve agents, in terms of its median lethal dose (LD_{50}), profile of inhibition of cholinesterases and general toxicity (9).

Acute OPC poisoning manifests itself with muscarinic effects (bronchoconstriction, bronchorroea, bradycardia, hypotension, nausea, vomiting, increased motility of bowels and bladder, miosis, hypersalivation, lacrimation), nicotinic effects (tachycardia, hypertension, fibrillation, fasciculations, skeletal muscle necrosis, mydriasis) and CNS effects (tremor, convulsions, coma, respiratory depression) (10). Intermediate syndrome can occur after 1–4 days and, 1–2 weeks later, organophosphate-induced delayed neuropathy (OPIDN) can be seen.

Treatment of OPC poisoning is based on a triple regimen: symptomatic anticholinergic therapy (atropine), AChE reactivators (oximes) and anticonvulsants (mainly diazepam) (11). Atropine as an antimuscarinic drug, alleviates the muscarinic effects of OPC poisoning, but has no impact on the nicotinic ones. Oximes bind to OPC already bound to AChE, which leads to the reactivation of AChE, with variable affinity for different OPCs between oximes. Diazepam inhibits the excitability of the neurons in the CNS; by increasing the effect of GABA, it increases cAMP, decreases the level of cGMP, leading to the cessation of convulsions (11).

The aim of the study was to analyse the clinical signs of acute paraoxon poisoning in rats and to determine whether there is a relationship between the intensity of toxicity signs and the dose of paraoxon and/or outcome of poisoning.

MATERIAL AND METHODS

ANIMALS

The study was conducted in adult Wistar rats weighing 200–240 g, purchased from the Faculty of Natural Sciences and Mathematics, University of Banja Luka, the Republic of Srpska. The animals were given water and food *ad libitum*, kept at a temperature of 20–22 °C, with a 12 h cycle of light and darkness. The study was approved by the Ethics Committee for the Protection and Welfare of Experimental Animals in Biomedical Research, Faculty of Medicine, University of Banja Luka (Decision No 18/1/20). The animals were treated in accordance with the Guide for the Care and Use of Laboratory Animals (12). The study was conducted at the Centre for Biomedical Research, Faculty of Medicine, University of Banja Luka.

CHEMICALS

Paraoxon was purchased from Sigma Aldrich, St Louis, MO, USA. Paraoxon was dissolved in isopropyl alcohol up to a concentration of 100 mg/mL and final dilution to the desired concentration was made with saline (0.9% NaCl). Atropine sulphate was dissolved in saline to a concentration of 10 mg/mL. The volumes of administered paraoxon and atropine were 1 mL/kg. Paraoxon and atropine were administered subcutaneously (sc) and intramuscularly (im), respectively. Final dilutions were made immediately before application.

STUDY DESIGN

The LD_{50} of paraoxon was determined by the "up and down" method according to Litchfield and Wilcoxon (1949) (13). In the first part of the experiment, then following doses of paraoxon were administered: 0.2, 0.3, 0.35, 0.4 mg/kg sc. One minute after paraoxon the saline (1 mL/kg, im) was administered. In the second part of the experiment, the following doses of paraoxon were administered: 0.6, 0.9 and 1.2 mg/kg sc. Atropine 10 mg/kg im was injected 1 minute after paraoxon application.

The presence and intensity of signs of paraoxon poisoning in animals were observed and recorded for 4 h. The following signs have been observed: dyspnoea, lacrimation, exophthalmos, fasciculations, tremor, ataxia, seizures, piloerection, stereotypic movements. Their presence and intensity were noted at the minutes: 5, 10, 15, 30, 60, 90, 120, 150, 180, 210 and 240 after paraoxon application. Intensity was evaluated as: 0 – absent, 1 – mild/moderate, 2 – severe. Signs of poisoning were observed in relation to the dose of paraoxon, as well as the outcome of the poisoning (survival or death).

Tab. 1 Time of death from paraoxon administration depending on paraoxon dose.

POX dose (mg/kg sc)		Time of death (minute)	
		Mean ± SD	95% CI
With saline	0.2	–	–
	0.3	16.67 ± 7.51	-1.98–35.31
	0.35	22.00 ± 3.61	18.67–25.33
	0.4	18.09 ± 6.99	13.39–22.78
	All	19.19 ± 6.19	16.37–22.01
With atropine	0.6	–	–
	0.9	14.00 ± 3.83	7.91–20.09
	1.2	14.00 ± 4.24	7.25–20.75
	All	14.00 ± 3.74	10.87–17.13
Total		**17.76 ± 6.04**	**15.46–20.06**

SD: standard deviation; CI: confidence interval; POX: paraoxon; Administered volumes of paraoxon, atropine and saline were 1 mL/kg; Atropine at a dose of 10 mg/kg im was given 1 minute after paraoxon application.

STATISTICS

The LD_{50} and the PR were analysed by the method of Litchfield and Wilcoxon (1949) on Pharm/PCS statistical software. Other analyses were performed on IBM SPPS for Windows, Version 18.0. After the Kolmogorov-Smirnov test showed an unequal distribution of data, appropriate nonparametric tests were applied: Chi-square test (or Fisher exact test) and Kruskal-Wallis test. Statistical significance level was set at $p < 0.05$.

RESULTS

The LD_{50} of paraoxon was 0.33 mg/kg sc (95% CI: 0.31–0.36). The LD_{50} of paraoxon when atropine was administered was 0.91 mg/kg sc (95% CI: 0.67–1.25). Therefore, the PR of atropine was 2.73. All deaths occurred during the first hour of poisoning (Table 1).

CLINICAL SIGNS OF POISONING

1. Fasciculations

Frequency of fasciculations was not correlated with the dose of paraoxon (Table 2).

In atropine-protected rats, fasciculations occurred more often in non-survivors ($p = 0.023$) (Table 3).

Fasciculations occurred earlier and were more intense at higher doses of paraoxon (Figure 1). Although the intensity of fasciculations were related to the dose of paraoxon throughout the observed period, the difference was significant in the minutes 10, 15, 30, 210 and 240 (Kruskal-Wallis test, $p = 0.035$, $p = 0.045$, $p = 0.038$, $p = 0.014$ and $p = 0.034$, respectively).

Due to atropine protection, higher doses of paraoxon could be administered. The intensity of fasciculations depending on paraoxon dose when atropine was administered is shown in Figure 2. Atropine did not influence the

Tab. 2 Frequency of signs of poisoning related to paraoxon dose.

Sign	Paraoxon + Saline						Paraoxon + Atropine				
	Paraoxon (mg/kg, sc)				Total	p*	Paraoxon (mg/kg, sc)			Total	p*
	0.2	0.3	0.35	0.4			0.6	0.9	1.2		
Fasciculations	100.00	66.67	100.00	83.33	85.71	0.080	100.00	83.33	50.00	77.78	0.250
Seizures	66.67	75.00	83.33	100.00	83.33	0.225	83.33	100.00	100.00	94.44	1.000
Tremor	83.33	100.00	100.00	100.00	97.61	0.143	100.00	100.00	100.00	100.00	1.000
Piloerection	0.00	33.33	66.67	75.00	50.00	**0.009**	50.00	50.00	0.00	33.33	0.149
Exophthalmos	83.33	91.67	100.00	100.00	95.23	0.498	83.33	100.00	100.00	94.44	1.000
Lacrimation	83.33	50.00	50.00	50.00	54.76	0.501	16.67	33.33	16.67	22.22	1.000
Ataxia	83.33	58.33	75.00	58.33	66.67	0.691	66.67	33.33	33.33	44.44	0.589
Stereotypy	100.00	66.67	83.33	41.67	69.05	**0.044**	66.67	0.00	50.00	38.89	0.095
Dyspnoea	33.33	33.33	25.00	16.67	26.19	0.862	50.00	50.00	33.33	44.44	1.000

* Chi-squared test (Fisher exact), **bold**: statistical significance. Values in the table are in percentages; sc: subcutaneously; im: intramuscularly; Administered volumes of paraoxon, atropine and saline were 1 mL/kg; Atropine at a dose of 10 mg/kg im was given 1 minute after paraoxon application.

Tab. 3 Frequency of signs of poisoning related to poisoning outcome.

Sign	Paraoxon + Saline				Paraoxon + Atropine			
	Rat survived		Total	p*	Rat survived		Total	p*
	Yes	No			Yes	No		
Fasciculations	85.71	85.71	85.71	1.000	50.00	100.00	77.78	**0.023**
Seizures	66.67	100.00	83.33	**0.009**	90.00	100.00	94.44	1.000
Tremor	95.23	100.00	97.61	1.000	100.00	100.00	100.00	1.000
Piloerection	23.81	76.19	50.00	**0.002**	40.00	25.00	33.33	0.638
Exophthalmos	95.23	95.23	95.23	1.000	90.00	100.00	94.44	1.000
Lacrimation	71.43	38.10	54.76	0.062	20.00	25.00	22.22	1.000
Ataxia	71.43	61.90	66.67	0.744	70.00	12.50	44.44	**0.025**
Stereotypy	85.71	52.23	69.05	**0.043**	60.00	12.50	38.89	0.066
Dyspnoea	28.57	23.81	26.19	1.000	60.00	25.00	44.44	0.239

* Chi-squared test (Fisher exact), **bold**: statistical significance; Values in the table are in percentages; im: intramuscularly; Administered volumes of paraoxon, atropine and saline were 1 mL/kg; Atropine at a dose of 10 mg/kg im was given 1 minute after paraoxon application.

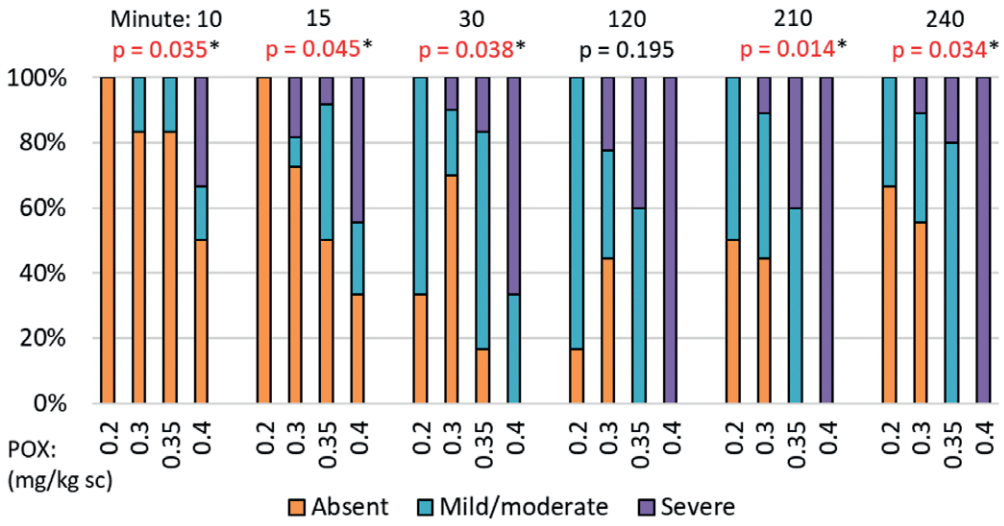

Fig. 1 Intensity of fasciculations in rats depending on paraoxon dose.
* Kruskal-Wallis test, red colour: statistical significance; POX: paraoxon; sc: subcutaneously; Minute: minutes 10, 15, 30, 120, 210 and 240 after paraoxon application.

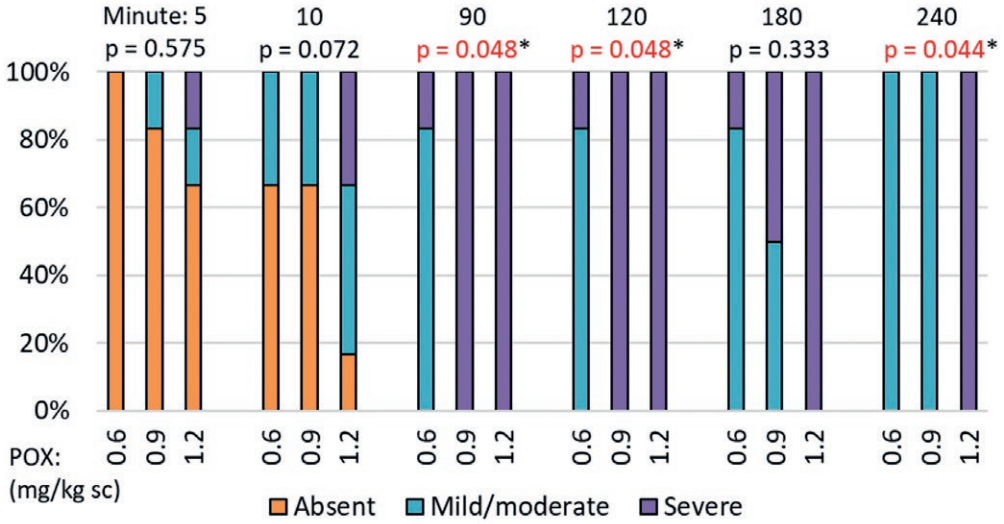

Fig. 2 Intensity of fasciculations depending on paraoxon dose in rats protected with atropine.
* Kruskal-Wallis test, red colour: statistical significance; POX: paraoxon; sc: subcutaneously; Minute: minutes 5, 10, 90, 120, 180 and 240 after paraoxon application; Atropine at a dose of 10 mg/kg im was given 1 minute after paraoxon application.

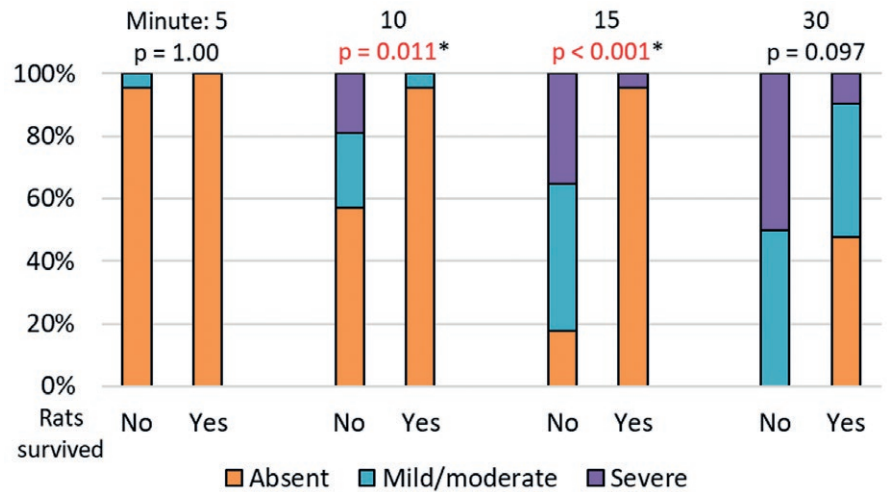

Fig. 3 Intensity of fasciculations in relation to whether rat treated with paraoxon survived or not.
* Fisher exact test, red colour: statistical significance; Minute: minutes 5, 10, 15 and 30 after paraoxon application.

intensity of fasciculations. Fasciculations occurred earlier and were more intense at higher doses of paraoxon. Although the intensity of fasciculations was related to the dose of paraoxon throughout the observed period, the difference was significant in the minute 60 (data not shown), 90, 120 and 240 (Kruskal-Wallis test, p = 0.033, p = 0.048, p = 0.048 and p = 0.044, respectively).

In unprotected rats intensity of fasciculations was in correlation with the outcome of poisoning (higher intensity was in non-survivors) (Figure 3). In atropine-protected rats, fasciculation intensity did not correlate with the outcome of poisoning.

2. Seizures

Frequency of seizures was not correlated with the dose of paraoxon (Table 2), but seizures were more often in non-survivors compared to survivors (Table 3). Seizures occurred earlier and were more intense at higher doses of paraoxon (Figure 4). Although the intensities of seizures were related to the dose of paraoxon throughout the observed period, the difference was significant only at minutes 15, 180 and 210 (Kruskal-Wallis test, p = 0.002, p = 0.024 and p = 0.015, respectively).

A clear relation between paraoxon dose and seizure intensity can be seen in atropine-protected rats (Figure 5). Although the intensity of seizures was related to the dose of paraoxon throughout the observed period, the difference was significant only at minutes 10, 15, 210 and 240 (Kruskal-Wallis test, p = 0.031, p = 0.014, p = 0.044 and p = 0.011, respectively).

In unprotected rats the intensity of seizures was in correlation with the outcome of poisoning (higher intensity was in non-survivors) (Figure 6). In atropine-protected rats, the intensity of seizures did not correlate with the outcome of poisoning.

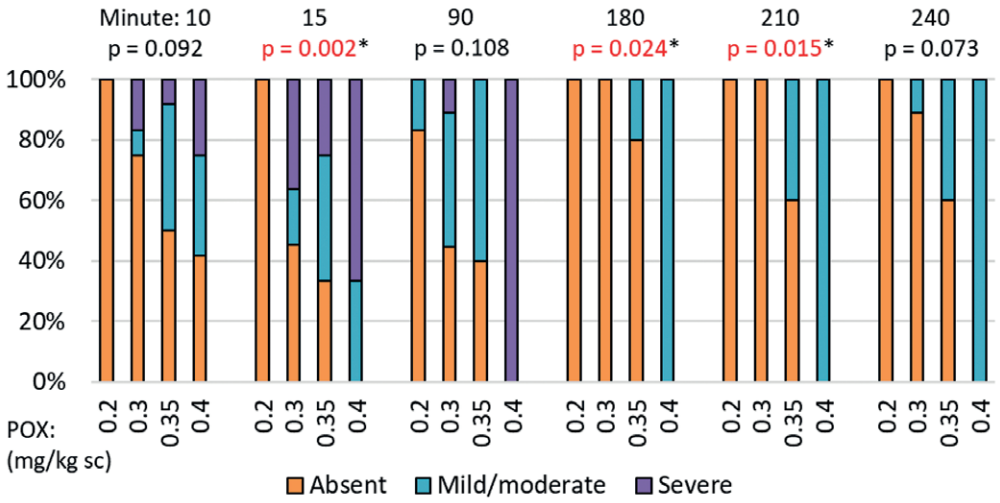

Fig. 4 Intensity of seizures in rats depending on paraoxon dose.
* Kruskal-Wallis test, red colour: statistical significance; POX: paraoxon; sc: subcutaneously; Minute: minutes 10, 15, 90, 180, 210 and 240 after paraoxon application.

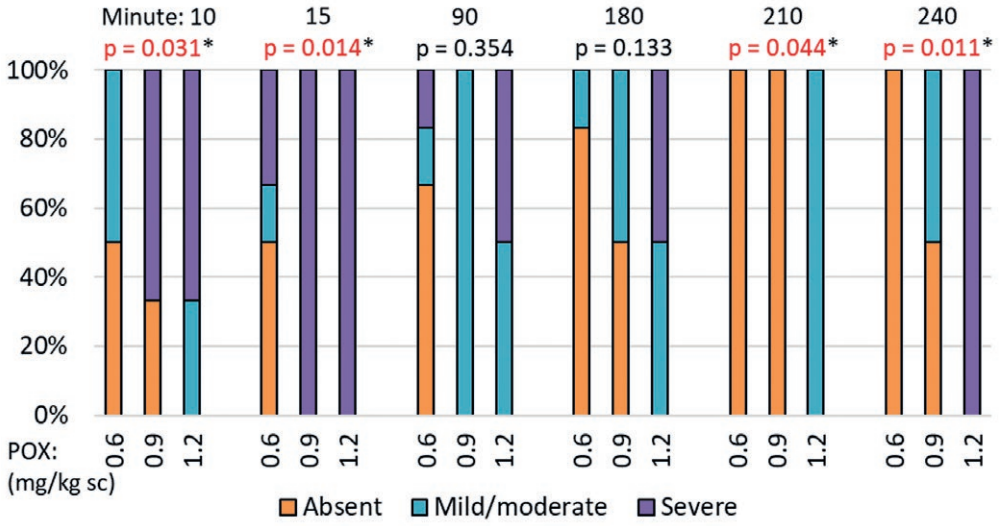

Fig. 5 Intensity of seizures depending on paraoxon dose in rats protected by atropine.
* Kruskal-Wallis test, red colour: statistical significance; POX: paraoxon; sc: subcutaneously; Minute: minutes 10, 15, 90, 180, 210 and 240 after paraoxon application; Atropine at a dose of 10 mg/kg im was given 1 minute after paraoxon application.

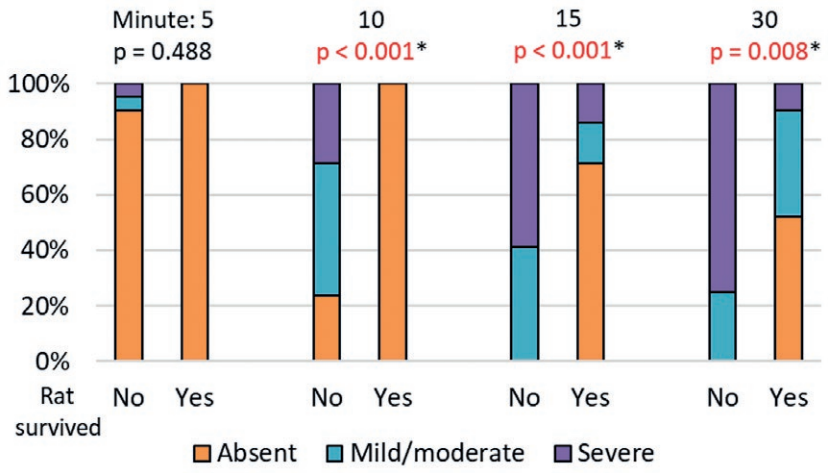

Fig. 6 Intensity of seizures in relation to whether rat treated with paraoxon survived or not.
* Fisher exact test, red colour: statistical significance; Minute: minutes 5, 10, 15 and 30 after paraoxon application.

3. Tremor

Frequency of tremor was not correlated with the paraoxon dose (Table 2) or the outcome of poisoning (Table 3). Tremor occurred earlier and was more intense at higher doses of paraoxon (Figure 7). Although the intensity of tremor was related to the dose of paraoxon throughout the observed period, the difference was significant at minutes 10, 15 and 240 (Kruskal-Wallis test, $p = 0.001$, $p = 0.002$ and $p = 0.044$, respectively).

In the atropine-protected rats, although a higher intensity of tremor was observed at higher doses of paraoxon, the difference was not significant, except at minute 10 ($\chi^2 = 9.88$, $p = 0.007$) and 30 ($\chi^2 = 6.00$, $p = 0.050$).

In unprotected rats intensity of tremor was in correlation with the outcome of poisoning (higher intensity was in non-survivors) (Figure 8). In atropine-protected rats, the intensity of tremor did not correlate with the outcome of poisoning.

4. Piloerection

Piloerection as a clinical sign of poisoning occurred early (within the first half hour of poisoning) and lasted for a short time (Figure 9). Piloerection occurred more often (Table 2) and was more intense at higher doses of paraoxon administered to unprotected rats. The difference was significant at minutes 10 and 15 (Kruskal-Wallis test, $p = 0.052$ and $p = 0.012$, respectively).

In atropine-protected rats, piloerection did not correlate with paraoxon dose.

In unprotected rats intensity of piloerection was in correlation with the outcome of poisoning. Piloerection was

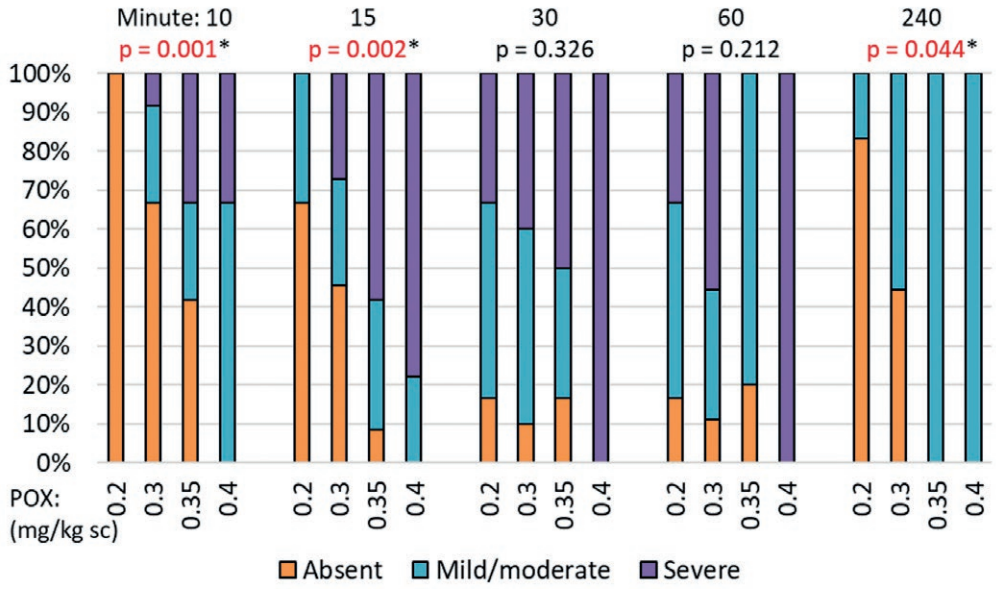

Fig. 7 Intensity of tremor in rats depending on paraoxon dose.
* Kruskal-Wallis test, red colour: statistical significance; POX: paraoxon; sc: subcutaneously; Minute: minutes 10, 15, 30, 60 and 240 after paraoxon application.

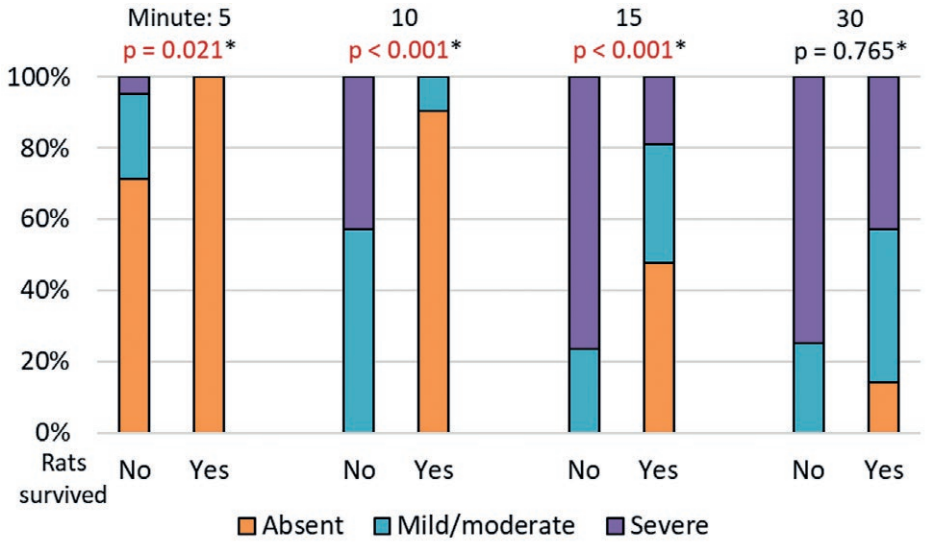

Fig. 8 Intensity of tremor in relation to whether rat treated with paraoxon survived or not.
* Fisher exact test, red colour: statistical significance; Minute: minutes 5, 10, 15 and 30 after paraoxon application.

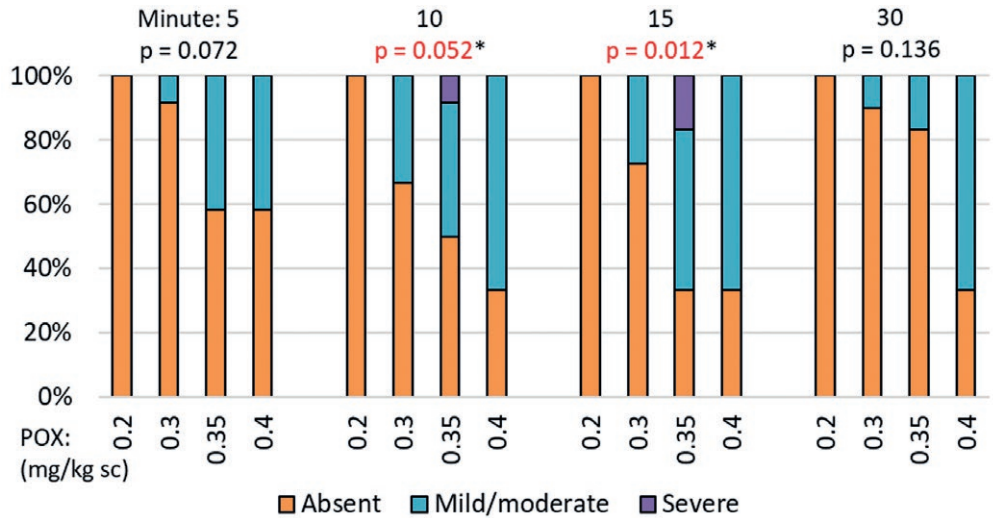

Fig. 9 Intensity of piloerection in rats depending on paraoxon dose.
* Kruskal-Wallis test, red colour: statistical significance; POX: paraoxon; sc: subcutaneously;
Minute: minutes 5, 10, 15 and 30 after paraoxon application.

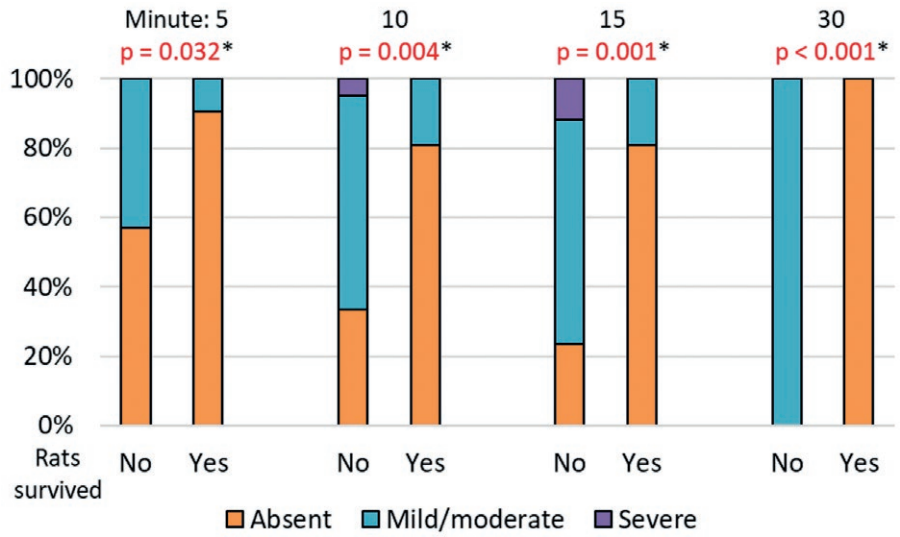

Fig. 10 Intensity of piloerection in relation to whether rat treated with paraoxon survived or not.
* Fisher exact test, red colour: statistical significance; Minute: minutes 5, 10, 15 and 30 after paraoxon application.

more often (Table 3) and of higher intensity in non-survivors (Figure 10). In atropine-protected rats, piloerection did not correlate with the outcome of poisoning.

The intensity of stereotypical movements, exophthalmos, lacrimation, ataxia and dyspnoea was not related to the dose of paraoxon or to the outcome of poisoning. The above results are not shown. Of the listed signs, stereotypical movements were less often with higher doses of paraoxon ($p = 0.044$) (Table 2). Related to poisoning outcome, ataxia ($p = 0.025$) was observed more often in survivors from the group of atropine-protected rats, while stereotypical movements ($p = 0.043$) were observed more often in survivors from the group of unprotected rats (Table 3).

DISCUSSION

Due to its extreme toxicity, the World Health Organization (WHO) has classified parathion, parent compound of paraoxon, as a class Ia (extremely hazardous) pesticide (14). Due to its toxicity, it is banned in most developed countries. Tabun, sarin, soman and VX represent OP compounds similar to parathion and paraoxon, with the same mechanism of action (inhibition of acetylcholinesterase) and their extreme toxicity classifies them as nerve agents. Their production, stockpiling, weaponosing and use is strictly prohibited by the 1993 Chemical Weapons Convention (CWC) (7). In undeveloped and developing countries, OPI poisonings, both accidental and intentional, are common (15, 16). In Sri Lanka and China, pesticide poisoning is the most common method of fatal self-harm (17).

The LD_{50} of paraoxon obtained in this study was 0.33 mg/kg sc, which corresponds with the results of other researchers (18). The PR of atropine was 2.73, which is in accordance with the known publications (19). Atropine is effective in blocking the effects of muscarinic but is ineffective against the nicotinic signs of OPC poisoning (20). This antimuscarinic drug is liposoluble and passes the blood-brain barrier (21). Therefore, it to some extent, antagonises the toxic effects of excessive cholinergic stimulation in the brain (22). It seems that a more lipophilic antimuscarinic drug would be more effective than atropine (23). Krutak-Krol and Domino (24) found that the atropine dose of 10 mg/kg im is optimal in experimental studies. The minimum absolute lethal dose of OPCs is 1.3 LD_{50} (25). The administration of atropine made it possible for rats to survive the absolute lethal dose of paraoxon. That enabled monitoring of signs of poisoning at high doses of paraoxon. As expected, atropine blocked to some extent the muscarinic effects, but not the nicotinic ones. Since different doses of paraoxon were administered in rats treated with saline or atropine, the results are not comparable. However, this makes it possible to compare the signs of poisoning in future studies with other antidotes.

In clinical settings, mainly muscarinic signs of OPC poisoning are expected. Bronchoconstriction and bronchorrhea are life-threatening muscarinic effects. Most studies have cited respiratory failure as the leading cause of death (26–28). Dyspnoea was observed as a sign of poisoning in the present experiment. No clear relationship was found between the intensity of dyspnoea and the dose of paraoxon. However, in the recent study, a clear relationship was found between the onset rate of dyspnoea, as well as the overall intensity of dyspnoea and lethal outcome of poisoning (29). Respiratory failure is a consequence of both peripheral and central cholinergic effects (30). Therefore, it is very important to administer an antidote that can cross the blood-brain barrier and prevent central respiratory depression (31).

Another muscarinic sign of poisoning that was observed is lacrimation. It is a sign that is easily noticeable. It is not a sign that directly implies whether the animal is endangered or not, but it is a good indicator of excessive muscarinic stimulation. In the treatment of OPC poisoning, the lack of lacrimation is one of the signs of achieving the so-called patient atropinisation (5). The results of this study also support this assumption. Although significantly higher doses of paraoxon were administered, the lacrimation occurred significantly less frequently in rats treated with atropine (22% vs 55%).

ACh is also found in the preganglionic nerve endings of the sympathetic nervous system (32). Stimulation of alpha-1-adrenergic receptors also leads to piloerection (33). Therefore, piloerection can serve as an indirect indicator of sympathetic stimulation. The results of this study showed a clear relationship between both the frequency and intensity of piloerection and the dose of paraoxon. Besides, piloerection occurred more often and was of stronger intensity in non-survivors.

Tachycardia and hypertension are rarely expected in patients with OPI intoxications and they often mislead physicians in practice. Saadeh et al found tachycardia in as many as 35–60% of patients poisoned by OPCs (34). It means that tachycardia occurs more often than bradycardia, which indicates that it is a prejudice not to expect nicotinic effects in OPC poisonings. Nicotinic signs of poisoning occur as a consequence of excessive stimulation of ganglionic nicotinic receptors (hypertension, tachycardia, diaphoresis) as well as receptors at the neuromuscular junction (fibrillation and fasciculation) (35). In AChEI poisoning, hypertension and tachycardia can also occur as a consequence of excessive stimulation of the *locus coeruleus*. Stimulation of this cholinergically innervated sympathetic nuclei leads to the centrally-originated hypertension (36, 37).

As already mentioned, ACh is a neurotransmitter of the peripheral nervous system, as well. Excessive stimulation of nicotinic receptors at the neuromuscular junction leads to fasciculations, a toxic phenomenon observed in this study. Fasciculations were the most consistent sign of the severity of rat poisoning. They were more intense at higher doses of paraoxon and in non-survivors throughout the observed period. This is in favour of the fact that nicotinic signs of poisoning appear in severe poisonings (38). When sarin was used in a terrorist attack in the crowded subway in Tokyo, over 5,000 people were injured and 12 people died (7, 39). Published reports cited nicotinic signs of poisoning in severely poisoned patients (40, 41). In rats treated with high doses of paraoxon and atropine, fasciculations were more common in survivors. This can be explained by the rapid lethal outcome of poisoning, which

left non-survivors without this toxic sign. Fasciculations often did not occur in the first 10 minutes of poisoning, but were present even after 4 hours in all survivors. In other words, it means that the non-survivors died too quickly to develop fasciculations. Experimental studies with antinicotinic drugs showed their significant antidotal efficacy against carbamates and OPCs (21). However, nicotinic receptor blockers are rarely used in clinical practice in the treatment of OPC poisonings, due to serious side effects at therapeutic doses of these drugs, primarily the respiratory muscle depression (42).

Tremor is mediated by a variety of neurotransmitters – dopamine, glutamate, serotonin, adenosine and acetylcholine (43). The M_2 muscarinic receptors are highly expressed in the nucleus basalis and occipital cortex, then in hippocampus and other cortical regions. Overstimulation of M_2 receptors leads to tremor (44). There is a conflicting evidence regarding the role of M_3 and M_4 receptors in tremor aetiology (45). In this study, a clear relationship was found between the intensity of poisoning, on the one hand and the dose of paraoxon and the outcome of the poisoning, on the other hand. In atropine-protected rats, tremor occurred in all animals. Tremor is often found as a part of the extrapyramidal syndrome that occurs as a consequence of permanent CNS damage in OPC poisoning survivors (21, 46, 47).

Stereotypical movements were registered more often in survivors and at lower dose of paraoxon. The heavily poisoned animals had significantly decreased spontaneous motor activity. Thus, the appearance of stereotypical movements could be a good prognostic sign of a positive outcome of poisoning. At the highest doses of paraoxon (0.9 and 1.2 mg/kg), ataxia was more common in survivors. Atropine prevented the death of rats, but not the skeletal muscle fatigue. As a consequence, only surviving rats could attempt to move in the cage and these movements were ataxic.

Seizures intensity was directly related to the dose of paraoxon and the lethal outcome of the poisoning. A total of 66.67% of survivors vs 100% of non-survivors had seizures. Seizures occur at the beginning of OPC poisoning due to the excessive cholinergic stimulation of the CNS. There are three treatment periods after the onset of OPC-induced convulsions: muscarinic, gamma-aminobutyric acid A ($GABA_A$)/benzodiazepine and glutamatergic ones (48). During the first one, antimuscarinic drugs (atropine and, preferably, more lipophilic drugs, such as scopolamine) can be efficiently used to stop the seizures, provided the right dose is chosen (49). However, beyond this period antimuscarinic drugs become ineffective in counteracting the seizures, irrespective of the dose applied. In the second phase this could be compensated by the administration of the $GABA_A$/benzodiazepine receptor antagonists, such as barbiturates (e.g., pentobarbital, thiopental sodium) and benzodiazepines (e.g., diazepam or midazolam) (50, 51). In the third phase, these seizures can be stopped by the administration of N-methyl-D-aspartate (NMDA) receptor antagonists, such as memantine, dizocilpine (MK-801) or ketamine (52–55). The reason for this is the fact that in the meanwhile the seizures became glutamatergic in its origin (56). Along with fasciculations, seizures were the most constant sign of the severity of the poisoning.

CONCLUSION

Among all the studied signs of paraoxon toxicity, the intensity of fasciculations and seizures were strong prognostic parameters of the severity of poisoning. They are easily observed and are directly related to both the dose of paraoxon and the lethal outcome of the poisoning. Based on the relationship between the frequency and intensity of muscarinic or nicotinic signs and the doses of paraoxon or outcomes of the poisoning, there are two strong prognostic parameters of the severity of poisoning (fasciculations and seizures) and a good prognostic sign of a positive outcome of poisoning (stereotypical movements). These signs of poisoning may be useful to researchers in monitoring the expected treatment outcome. Also, the appearance of nicotinic and central signs of poisoning in patients indicates the severity of poisoning and provides guidance to clinicians on which potential therapy to use.

FUNDING

This study is partially funded by the Ministry of Scientific and Technological Development, Higher Education and Informational Society of the Government of the Republic of Srpska (Grant No 125 7030).

ABBREVIATIONS

ACh: acetylcholine; AChE: acetylcholinesterase; AChEI: acetylcholinesterase inhibitor; OPC: organophosphorus compounds; OPI: organophosphate insecticide

REFERENCES

1. Brown DA. Acetylcholine and cholinergic receptors. Brain Neurosci Adv 2019 Mar 21; 3: 2398212818820506.
2. Pope CN, Brimijoin S. Cholinesterases and the fine line between poison and remedy. Biochem Pharmacol 2018 Jul; 153: 205–16.
3. Xiao C, Zhou CY, Jiang JH, Yin C. Neural circuits and nicotinic acetylcholine receptors mediate the cholinergic regulation of midbrain dopaminergic neurons and nicotine dependence. Acta Pharmacol Sin 2020 Jan; 41(1): 1–9.
4. Vale A, Lotti M. Organophosphorus and carbamate insecticide poisoning. Handb Clin Neurol 2015; 131: 149–68.
5. Eddleston M. Novel clinical toxicology and pharmacology of organophosphorus insecticide self-poisoning. Annu Rev Pharmacol Toxicol 2019 Jan 6; 59: 341–60.
6. Henretig FM, Kirk MA, McKay CA Jr. Hazardous chemical emergencies and poisonings. N Engl J Med 2019 Apr 25; 380(17): 1638–55.
7. Stojiljković MP. Nerve agents – a clear and present danger to mankind. Scr Med 2019; 50(3): 109–11.
8. Lorke DE, Nurulain SM, Hasan MY, Kuča K, Petroianu GA. Combined pre- and posttreatment of paraoxon exposure. Molecules 2020 Mar 27; 25(7): 1521.
9. Wadia RS, Sadagopan C, Amin RB, Sardesai HV. Neurological manifestations of organophosphate insecticide poisoning. J Neurol Neurosurg Psychiatry 1974 Jul; 37(7): 841–7.
10. Reddy BS, Skaria TG, Polepalli S, et al. Factors associated with outcomes in organophosphate and carbamate poisoning: a retrospective study. Toxicol Res 2020 Feb 7; 36(3): 257–66.

11. Amend N, Niessen KV, Seeger T, Wille T, Worek F, Thiermann H. Diagnostics and treatment of nerve agent poisoning-current status and future developments. Ann N Y Acad Sci 2020 Nov; 1479(1): 13–28.
12. National Research Council (US) Committee for the Update of the Guide for the Care and Use of Laboratory Animals. Guide for the Care and Use of Laboratory Animals. 8th edition. Washington (DC): National Academies Press (US); 2011. Available from: https://www.ncbi.nlm.nih.gov/books/NBK54050/.
13. Litchfield JT Jr, Wilcoxon F. A simplified method of evaluating dose-effect experiments. J Pharmacol Exp Ther 1949 Jun; 96(2): 99–113.
14. WHO. The WHO recommended classification of pesticides by hazard 2019. Geneva, 2019. (Accessed 2021-May-02 at https://apps.who.int/iris/bitstream/handle/10665/332193/9789240005662-eng.pdf?ua=1.)
15. Amir A, Raza A, Qureshi T, et al. Organophosphate poisoning: demographics, severity scores and outcomes from National Poisoning Control Centre, Karachi. Cureus 2020 May 31; 12(5): e8371.
16. Kaushal J, Khatri M, Arya SK. A treatise on organophosphate pesticide pollution: Current strategies and advancements in their environmental degradation and elimination. Ecotoxicol Environ Saf 2020 Oct 22; 207: 111483.
17. WHO. Health topics: mental health. Geneva, 2004. (Accessed 2021-May-02 at https://www.who.int/mental_health/prevention/suicide/en/PesticidesHealth2.pdf.)
18. Misik J, Pavlikova R, Cabal J, Kuca K. Acute toxicity of some nerve agents and pesticides in rats. Drug Chem Toxicol 2015 Jan; 38(1): 32–6.
19. Holmstedt B. Pharmacology of organophosphorus cholinesterase inhibitors. Pharmacol Rev 1959 Sep; 11: 567–688.
20. Parkes MW, Sacra P. Protection against the toxicity of cholinesterase inhibitors by acetylcholine antagonists. Br J Pharmacol Chemother 1954 Sep; 9(3): 299–305.
21. Stojiljković MP, Škrbić R, Jokanović M, Kilibarda V, Bokonjić D, Vulović M. Efficacy of antidotes and their combinations in the treatment of acute carbamate poisoning in rats. Toxicology 2018 Sep 1; 408: 113–24.
22. Kords H, Lüllmann H, Ohnesorge FK, Wassermann O. Action of atropine and some hexane-1.6-bis-ammonium derivatives upon the toxicity of DFP im mice. Eur J Pharmacol 1968 Jul; 3(4): 341–6.
23. Albuquerque EX, Pereira EF, Aracava Y, et al. Effective countermeasure against poisoning by organophosphorus insecticides and nerve agents. Proc Natl Acad Sci U S A 2006 Aug 29; 103(35): 13220–5.
24. Krutak-Krol H, Domino EF. Comparative effects of diazepam and midazolam on paraoxon toxicity in rats. Toxicol Appl Pharmacol 1985 Dec; 81(3 Pt 1): 545–50.
25. Antonijević B, Stojiljković MP, Bokonjić D, Vucinić S. [Antidotal effect of combinations obidoxime/HI-6 and memantine in mice poisoned with soman, dichlorvos or heptenophos]. Vojnosanit Pregl 2011 Dec; 68(12): 1033–40. Serbian.
26. Eddleston M, Eyer P, Worek F, et al. Differences bet organophosphorus insecticides in human self-poisoning: a prospective cohort study. Lancet 2005 Oct 22–28; 366(9495): 1452–9.
27. Namba T, Nolte CT, Jackrel J, Grob D. Poisoning due to organophosphate insecticides. Acute and chronic manifestations. Am J Med 1971; 50(4): 475–92.
28. Ballantyne B, Marrs TC. Overview of the biological and clinical aspects of organophosphates and carbamates. In: Ballantyne B, Marrs TC, eds. Clinical and experimental toxicology of organophosphates and carbamates. Oxford: Butterworth-Heinemann; 1992, p. 3–14.
29. Maksimović ŽM, Duka D, Bednarčuk N, Škrbić R, Stojiljković MP. Onset rate and intensity of signs of organophosphate poisoning related to paraoxon dose and survival in rats. Scr Med 2021 Mar; 52(1): 49–58.
30. Villa AF, Houze P, Monier C, et al. Toxic doses of paraoxon alter the respiratory pattern without causing respiratory failure in rats. Toxicology 2007 Mar 22; 232(1–2): 37–49.
31. Houze P, Pronzola L, Kayouka M, Villa A, Debray M, Baud FJ. Ventilatory effects of low-dose paraoxon result from central muscarinic effects. Toxicol Appl Pharmacol 2008 Dec 1; 233(2): 186–92.
32. Dhanarisi J, Shihana F, Harju K, et al. A pilot clinical study of the neuromuscular blocker rocuronium to reduce the duration of ventilation after organophosphorus insecticide poisoning. Clin Toxicol (Phila) 2020 Apr; 58(4): 254–6.
33. Kikuchi-Utsumi K, Ishizaka M, Matsumura N, Nakaki T. Alpha(1A)-adrenergic control of piloerection and palpebral fissure width in rats. Auton Neurosci 2013 Dec; 179(1–2): 148–50.
34. Saadeh AM, Farsakh NA, al-Ali MK. Cardiac manifestations of acute carbamate and organophosphate poisoning. Heart 1997; 77(5): 461–4.
35. Turner SR, Chad JE, Price M, et al. Protection against nerve agent poisoning by a noncompetitive nicotinic antagonist. Toxicol Lett 2011 Sep 25; 206(1): 105–11.
36. Dirnhuber P, Cullumbine H. The effect of anti-cholinesterase angents on the rat's blood pressure. Br J Pharmacol Chemother 1955 Mar; 10(1): 12–5.
37. Varagić V. The action of eserine on the blood pressure of the rat. Br J Pharmacol Chemother 1955 Sep; 10(3): 349–53.
38. Persson HE, Sjöberg GK, Haines JA, Pronczuk de Garbino J. Poisoning severity score. Grading of acute poisoning. J Toxicol Clin Toxicol 1998; 36(3): 205–13.
39. Yokoyama K, Yamada A, Mimura N. Clinical profiles of patients with sarin poi¬soning after the Tokvo subway attack. Am J Med 1996 May: 100(5): 586.
40. Nozaki H, Aikawa N, Shinozawa Y, Hori S, Fujishima S, Takuma K, et al. Sarin poisoning in Tokyo subway. Lancet 1995 Apr 15: 345(8955): 980–1.
41. Suzuki T, Morita H, Ono K, Maekawa K, Nagai R, Yazaki Y. Sarin poisoning in To¬kyo subway. Lancet 1995 Apr 15; 345(8955): 980.
42. Sheridan RD, Smith AP, Turner SR, Tattersall JE. Nicotinic antagonists in the treatment of nerve agent intoxication. J R Soc Med 2005 Mar; 98(3): 114–5.
43. Collins LE, Galtieri DJ, Brennum LT, et al. Oral tremor induced by the muscarinic agonist pilocarpine is suppressed by the adenosine A2A antagonists MSX-3 and SCH58261, but not the adenosine A1 antagonist DPCPX. Pharmacol Biochem Behav 2010 Feb; 94(4): 561–9.
44. Gomeza J, Shannon H, Kostenis E, et al. Pronounced pharmacologic deficits in M_2 muscarinic acetylcholine receptor knockout mice. Proc Natl Acad Sci U S A 1999 Feb 16; 96(4): 1692–7.
45. Scarr E. Muscarinic receptors: their roles in disorders of the central nervous system and potential as therapeutic targets. CNS Neurosci Ther 2012 May; 18(5): 369–79.
46. Jokanović M. Neurotoxic effects of organophosphorus pesticides and possible association with neurodegenerative diseases in man: A review. Toxicology 2018 Dec 1; 410: 125–31.
47. Reji KK, Mathew V, Zachariah A, et al. Extrapyramidal effects of acute organophosphate poisoning. Clin Toxicol (Phila) 2016 Mar; 54(3): 259–65.
48. Stojiljković MP, Jokanović M, Lončar-Stojiljković D, Škrbić R. Prophylactic and therapeutic measures in nerve agents poisonings. In: Gupta RC. Handbook of toxicology of chemical warfare agents. 3rd ed. Cambridge, MA, USA: Academic Press; 2020, p. 1145–1159.
49. Myhrer T, Nguyen NH, Andersen JM, Aas P. Protection against soman-induced seizures in rats: relationship among doses of prophylactics, soman, and adjuncts. Toxicol Appl Pharmacol 2004 May 1; 196(3): 327–36.
50. Shih T, McDonough JH Jr, Koplovitz I. Anticonvulsants for soman-induced seizure activity. J Biomed Sci 1999 Mar–Apr; 6(2): 86–96.
51. Bokonjić D, Rosić N. Anticonvulsive and protective effects of diazepam and midazolam in rats poisoned by highly toxic organophosphorus compounds. Arh Hig Rada Toksikol 1991 Dec; 42(4): 359–65.
52. Spampanato J, Bealer SL, Smolik M, Dudek FE. Delayed adjunctive treatment of organophosphate-induced status epilepticus in rats with phenobarbital, memantine, or dexmedetomidine. J Pharmacol Exp Ther 2020 Oct; 375(1): 59–68.
53. Stojiljković MP, Škrbić R, Jokanović M, Bokonjić D, Kilibarda V, Vulović M. Prophylactic potential of memantine against soman poisoning in rats. Toxicology 2019 Mar 15; 416: 62–74.
54. Weissman BA, Raveh L. Therapy against organophosphate poisoning: the importance of anticholinergic drugs with antiglutamatergic properties. Toxicol Appl Pharmacol 2008 Oct 15; 232(2): 351–8.
55. Stojiljković MP, Škrbić R, Jokanović M, Kilibarda V, Bokonjić DR, Maksimović M. Effects of memantine and its metabolite Mrz 2/373 on soman-induced inhibition of acetylcholinesterase in vitro. Chem Biol Interact 2021 Jun 1; 342: 109463.
56. Rusyniak DE, Nañagas KA. Organophosphate poisoning. Semin Neurol 2004 Jun; 24(2): 197–204.

Contactless Measurement of Integrity of Silicone Coating on Self-Expandable Esophageal Nitinol Stents

Martin Kopeček[1,*], Jiří Záhora[1], Aleš Bezrouk[1]

ABSTRACT

Objectives: A stent is a mesh tube inserted into a natural passage in the body to prevent disease induction. Self-expandable esophageal nitinol stents such as SX-ELLA Stent Esophageal HV (HV Stent Plus) can be indicated for palliation of malignant esophageal strictures, for the treatment of benign esophageal strictures that are refractory to standard therapy and for the treatment of esophago-respiratory fistulas. A silicone-stent coating is used for tumor in-growth prevention and esophago-respiratory fistula occlusion. The thickness of the stent and the overall integrity of the silicone coating of all wires indicate the overall mechanical properties of the esophageal stent and the resistance to external adverse events such as corrosion and mechanical and chemical resistance.

Methods: The polymer multicomponent epoxy resin – a mixture of Epon and Durcupan – was used as a method for robust sample stabilization. A cutting system using a thin water beam with a powder (Blue Line) was chosen as the best variant to obtain 6 samples for both-sided measurement (10 measuring sides). The optical microscopic reflective light method was used to examine wire crossing points in the sections. Fifty values were measured on either sample side for the internal, external and mesh thickness of the silicone stent layer. The wire crossing points were selected so that the silicone layer structure could be clearly seen, and the wires approached each other most closely. Only approximately 4 to 8 crossing points in each section could be measured when applying this approach. The resolution of the microscope and calibration (based on the camera used) was 0.677 µm/pixel.

Results: Additional data could be obtained on 8 planes. Two boundary samples were destroyed by the cutting process. Whole coating of the stent was around all mesh wires, especially in areas with higher mechanical stress (wire crossing). The minimum detectable and admissible value determined for all 3 measuring areas (internal, external, mesh) on the wire crossings was 6.77 µm, i.e., 10 pixels, based on the microscope resolution and manufacturer's methodology. The results were characterized by $p < 0.001$ for all 3 parameters. We tested opposite samples in each section to verify the section quality and data consistency. For the 4 areas, the data were significantly different, but the thickness differences were only on the order of units percent, so the measurements were not appreciably affected. We assume that the material cutting loss, making up 1–2 mm, contributed to the differences in the sections.

Conclusion: We examined the overall integrity of the silicone coating of the esophageal stent. The method of HV stent anchoring in a polymeric bath followed by cutting with a waterjet and sample measurement under an optical microscope proved to be very simple and reliable. Sufficient thicknesses of the silicone layer on the wire cross sections were verified. The coated silicone layer thickness appeared to be significantly different along the stent from the proximal part to the distant part, presumably due to the manufacturing technology.

KEYWORDS

nitinol; stent; self-expandable; memory materials; CNC technology; epoxy resin; contactless; optical method; silicone coating

AUTHOR AFFILIATIONS

[1] Department of Medical Biophysics, Charles University, Faculty of Medicine in Hradec Králové, Hradec Králové, Czech Republic

* Corresponding author: Department of Medical Biophysics, Charles University, Faculty of Medicine in Hradec Králové, Šimkova 870, 500 03 Hradec Králové, Czech Republic; e-mail: kopecema@lfhk.cuni.cz

Received: 22 November 2021
Accepted: 23 March 2022
Published online: 29 June 2022

Acta Medica (Hradec Králové) 2022; 65(1): 18–24
https://doi.org/10.14712/18059694.2022.11

INTRODUCTION

Self-expandable nitinol stents are made of a metal alloy of nickel and titanium (TiNi 50%) with specific properties, such as shape memory, hyperelasticity, superelasticity, and biocompatibility, that are useful for medical applications, especially for long-term use. The problem is that a tumor can easily penetrates through the stent mesh and the esophageal liquids cause the mesh corrosion. Prevention of tumor in-growth and occlusion of esophagorespiratory fistulas can be achieved by a silicone coating (1). In case of a faulty coating, nitinol wires may contact tissue and cause serious problems with the introduction and use of HV Stent Plus. Over time, the uncovered portion of the nitinol stents could be expanded. The tear of the protective silicone layer could be ruptured and start occlusion in the esophagus-respiratory fistula (2, 3).

Morphological properties and coating thickness were mostly monitored by scanning electron microscopy (SEM) (4, 5). The great advantage of this observation method is that it is very accurate and there is a good contrast of the silicone layer to the background. However, a major disadvantage is a way of cutting the nitinol wire, where the silicone is moved along the wire when the stent is deployed.

To eliminate deformations caused by stent division due to different physical properties of the nitinol stent and the coating, we proposed a method using embedding the stent in resin and subsequent cutting of the sample using a water jet with an abrasive powder. In this paper, we present the results of using this method to measure an HV Stent Plus by an optical microscopy method. Our method tries to verify the integrity of the protective silicone layer of nitinol wires, their crossing, and the space of the mesh windows too (6). The covering of the HV Stent Plus is made of durable silicone and ELLA-CS manufactures all its stent silicone covers in the same way. The mandrel with the stent attached to it rotates around its own axis at a predefined constant speed. The injection needle moves along the surface of the stent at a predefined height in one direction – from the proximal to the distal part. The speed of movement and delay time at the beginning and end of the procedure can be changed, as can the total amount of silicone applied.

No unambiguous conclusions have been reached to date concerning the adequacy of stent skeletons covered with silicone for this stent type. These parameters are under investigation and are important for the verification of production processes.

In our study, we present a new method using the optical microscope to measure thickness and detect failures in silicone coating of nitinol stents. This issue has not yet been addressed by scientific attention in detail (7), and the solution described in this work is unique and original.

MATERIAL AND METHODS

We used commercially available SX-ELLA Stent Esophageal HV – HV Stent Plus (Fig. 1) made from nitinol alloy with silicone coating for the in vitro tests. Stent (Fig. 1) was 85 mm long (*LN*), 25 mm in diameter at the stent flares (*D1*) and 20 mm at the middle of the stent (*D2*).

The method is based on the three general steps. The laboratory compounds and chemical preparation of the sample are described in the first part. A multicomponent epoxy resin was used as a supporting fixative medium. In the second part, the method describes the CNC technology for high-pressure waterjet material division of the stent without destroying the silicone layer (8–10). The last, most important part describes the process of measuring the integrity of the silicone coating by an optical motorized advanced research microscope. The primary outcomes are evaluation of the laboratory protocol and verification of the accuracy of the manufacturing process.

Several methods were proposed to measure the thickness of the silicone coating of the esophageal HV Stent Plus (11), but it was not possible to objectively evaluate the accuracy of the measurements – it was not possible to compare the measured values with other physical quantities. Therefore, the optical measurement method with the Nikon Eclipse 90i and NIS-Elements AR 3.20 – Imaging Software was selected for our precise measurement. The soaking or deposition system for mandrel rotation induces targeted inhomogeneity in the thickness of silicone with different geometries of the proximal and distal portions. A rapid quantitative evaluation of a homogeneous surface

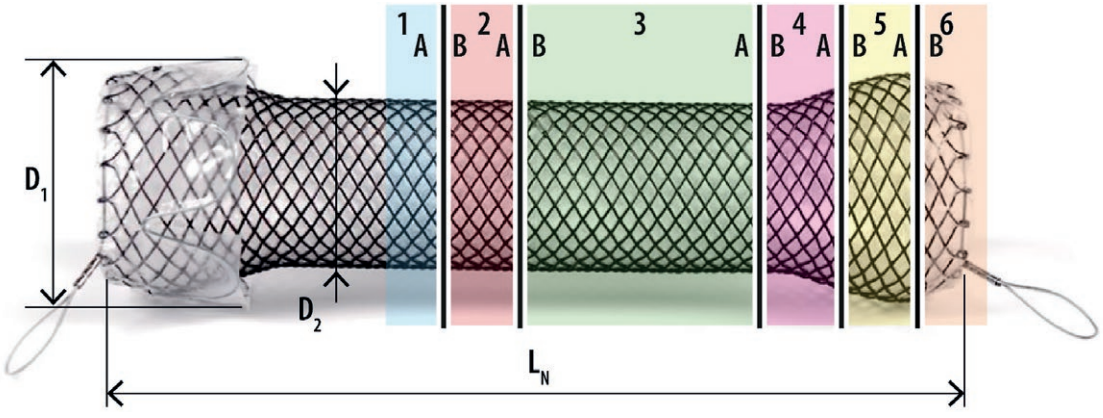

Fig. 1 Slices of areas in HV Stent Plus. The numbers with colored parts are samples, and each sample has two sides. The stent passes from the left-hand proximal part to the right-hand distal part.

coating is the goal of many manufacturers. This connection of cleverly applied methodology with the applied sphere is very desirable.

A. SAMPLE POLYMERIZATION

HV Stent Plus was cut into several sections, as shown in Fig. 1, to measure the thickness of the silicone layer. Thanks to this process, it was possible to measure the thickness at different sites of the HV Stent Plus and at various wire intersections. The initial intention was to cut the HV Stent Plus with special shears, but the wires would roll out and the HV Stent Plus would lose its shape. Cutting the sample preparation with the shears resulted in the HV Stent Plus rolling out, and the integrity of the silicone with the wires was compromised. It was also inappropriate to use deep freezing and subsequent cutting with a laboratory grinder. In these experiments, the silicone layer was torn and could not be kept in direct contact with the wire.

There was only one right option to avoid destroying the material and still have a smooth cut. HV Stent Plus was embedded into a plastic laboratory measuring cylinder and soaked in resin. HV Stent Plus was embedded by using multicomponent epoxy resin – a mixture of Epon and Durcupan ACM (12). (One component is Epon 812 (13), and the other three are durcupan series). The compound was mixed for approximately 40 minutes by an electromagnetic shaker. After embedding (in our case – in the truncated plastic cylinder), the specimen was left for 3 days with a thermostat set at 60 °C, which made the final polymerization of the resin. This method of preparation is unique in the area of stent measurement. Cured epoxy resin without air bubbles acts as a support material.

B. SLICING

An abrasive waterjet cutting method was used for the preparation of the samples. Cutting (10, 14) was performed using CNC technology for high-pressure waterjet material division (Blue Line – Rychly TOM Ltd. Company) with a positioning precision of 0.02 mm, as is partly described in (15). The quality (precision) approached that attained by conventional machining. A beam of high-pressure water with the addition of abrasives is used for controlled grinding of a particular material. Owing to the principle of this technology, the material is unaffected by any thermal effects, in contrast to other applicable cutting methods (laser, plasma, oxyfuel cutting). The cutting gap thickness when using a hydroabrasive beam is between 0.8 mm and 2.5 mm. The sample cutting procedure involves minimum jet force acting on the material, no microcracks are formed and a high-quality cut, free from burrs, is obtained. This helped create smooth cuts where the nitinol wires (16), silicone and support resin were not mostly destroyed, as shown in Figure 2.

Fig. 2 Layer integrity of the nitinol wire, silicone coating and resin after waterjet cutting.

C. CONTACTLESS MEASUREMENT METHOD

Samples were selected that were qualitatively appropriate and usable, and for which it was possible to distinguish individual layers in the cut. Their final selection is shown in Fig. 1. Using an optical microscope, the thickness of the silicone layer was gradually measured at 5x magnification. The final image was measured as shown in Fig. 3. In (17), the authors demonstrate uniform density and integrity of the silicone covering nitinol stent arms and coat the stent wire mesh even at wire crossings. It can be assumed that the wire was cut crosswise during sample preparation; however, for a general view of the stent, we cannot determine from the study whether this silicone is indeed uniformly applied everywhere. We take these facts into account and broaden our knowledge of the properties of the HV Stent Plus coating by using the optical method with a high observed data density.

All the important and evaluable areas were selected at each cut and measured by our optical method. Therefore, we obtained a large amount of data for different distances between wires (wire spacing – mesh) and internal and external thicknesses for silicone around wires, as shown in Fig. 4. The results could be further processed statistically for a large amount of data.

The first step was to determine the minimum silicone layer thickness. We used a Nikon LU Plan Fluor 5x/0.15 objective with a resolution of 0.278 μm. The resolution obtained by combination with the DSFI1 camera was 0.677 μm/pixel based on the manufacturer's calibration. We set the minimum silicone layer thickness at 10 times the microscope resolution, i.e., 6.77 μm to ensure that we have available an adequately wide range of silicone layer thicknesses evaluable by the conventional method.

Therefore, 6.77 μm is the minimum detectable layer thickness for which we can determine if the silicone coating is present at the point measured. In other words, we can decide whether the wire is fully silicone-coated. The manufacturer does not have the specified minimum thickness of the applied layer, and there is no standard for this. The ideal thickness of silicone is based only on the manufacturer's technological procedures with emphasis on the distribution of mechanical forces inside the HV Stent Plus.

The measurement of the samples was the second step. The silicone layer was sometimes difficult to read, but the number of wires was large enough to enable areas suitable for measurement to be selected. Thanks to cutting possibilities, 4 samples could be made to measure at both sides. Samples 1 and 6 could not be measured due to destruction during cutting. The applicable samples were described

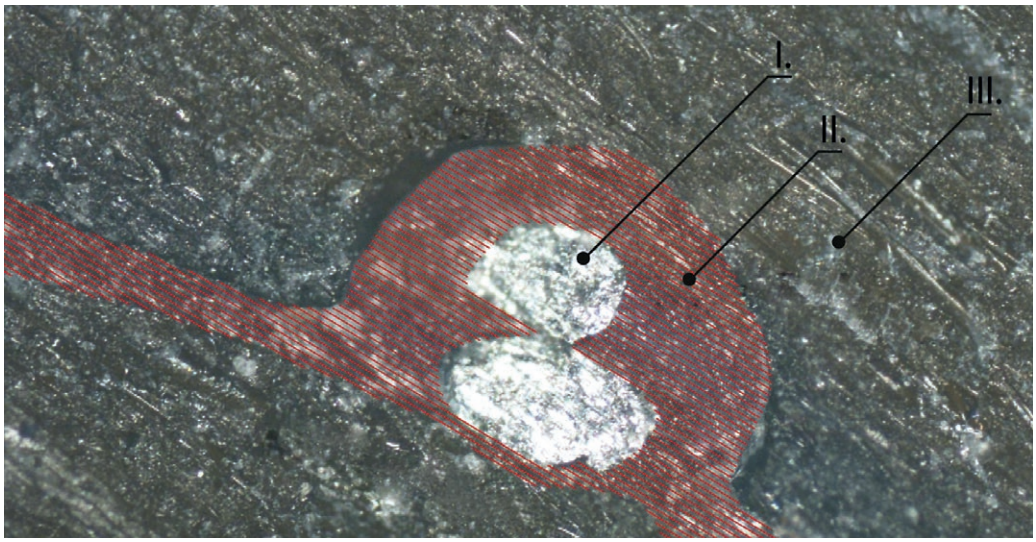

Fig. 3 I is the nitinol wire, II is the silicone layer area around the wire and III is the cured resin. The data define the silicone thickness between the wires.

from both sides and then divided into three groups. Group I includes the values of the 2BA and 3BA sections, samples 4BA and 5B were included in Group II and 5A in Group III. In total, there were 8 plate sides for measurement, and approximately 10 (Fig. 2) crossing wire samples were processed on each side. Four to eight wire crossings from each side were measured 7–10 times (Fig. 4). Number of readings depended on the recognition quality of the silicone/polymer boundary. We decided to measure a total of 50 silicone thickness values at all wire crossings on either side of the section. The details of the crossing of the wire and example of the measurements are shown in Fig. 4.

D. STATISTICAL ANALYSIS

The external, internal, and mesh coating thicknesses of the corresponding sides of each section were statistically compared using MS Excel 2016 (Microsoft Corp., Redmond, WA, USA) and NCSS 12 (NCSS LLC, Kaysville, UT, USA, ncss.com/software/ncss). We used the D'Agostino omnibus test to test the normality of the data distribution. The data from normally distributed populations were then described using the mean and standard deviation of the sample (± SD), while the other data were described using the median and the first and third quartiles of (1st Q, 3rd Q). Since the normality of the distribution of the same shoulder area data was rejected, we opted to use the Wilcoxon signed-rank test because it does not presuppose a normal distribution. A value of $p < 0.05$ was considered to be significant.

RESULTS AND DISCUSSION

The support resin exhibited negative coloring properties. The epoxy resin did not sufficiently contrast with the

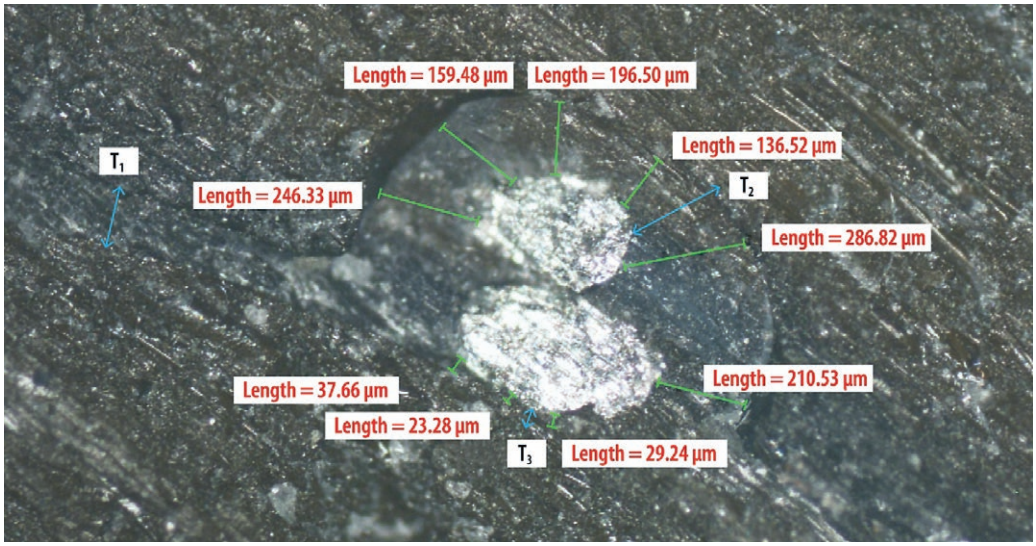

Fig. 4 Three parameters at the cross wire cut. T_1 shows mesh thickness – thickness of the silicone between two wires. T_2 is external thickness – the outside part and T_3 is internal thickness – the inside part of the HV Stent Plus

measured sample, so measurement was difficult at certain points. Additionally, the silicone layer partially absorbed the resin. Sometimes it caused worse readability of the results, sometimes the problem was with poor quality of a section, which affected the image sharpness, and sometimes the section failed to precisely include a wire crossing. Such areas were excluded from measurement. However, it was mostly clear where the boundary between the polymer and the stent was (18). Although HV Stent Plus was precisely laboratory-embedded in the resin, occasionally, despite careful degreasing, it was not possible to directly bond the resin to the silicone layer. This is also evident in Fig. 3, where the silicone layer is not directly in contact with the support. This phenomenon had no effect on the measurement. This is only an effect of insufficient strength of the silicone layer with the resin during the slicing process.

The statistics are borderline. With a larger number of data for only one HV Stent Plus, a greater significance of the differences would be more likely to be achieved. However, the developed method is still acceptable for the intended use in practice. More samples could not be obtained due to the cutting technology used. The stent attachment method in the waterjet cutting machine did not allow for multiple incisions, and no other HV Stent Plus of the same type was available to increase testing. We assume that the manufacturer produces these stents according to standards and certifications of the highest quality. A new stent intended for use in surgery, after passing factory output inspection, was used for the testing. Based on those criteria and regular internal testing by the manufacturer, we believed the stents would have the same properties as the tested product. The deviation is due to the manual stent weaving process because the total surface area of the skeleton material is not constant; hence, the thickness of the silicone layer, the volume of which is always the same for a stent size, may differ by units percent.

The results in Fig. 5 of the silicone coating thickness in the wire intersection show that the minimal measured value of 11.6 μm was significantly greater than the minimum acceptable thickness given by imaging method parameters – a resolution of 0.677 μm for the microscope and above the minimum value of the verification method of 6.77 μm set by us. The presence of silicone was confirmed by our method for all sections and for all three monitored parameters as internal, external and mesh thickness ($p < 0.001$).

Since we tested the selected sample preparation/cutting method, we made a statistical comparison of the two sides of each section. Statistically significant differences in the silicone coating thicknesses were only identified for the sides of Section 4A vs. 5B ($p < 0.001$) (internal, external and mesh thicknesses) and Section 2A vs. 3B ($p = 0.028$) (mesh thickness). Presumably, the silicone layer thicknesses are different due to the coarse cut with the waterjet-powder system, as a result of which the material is partly damaged, and the layer is not as smooth as the undisturbed side. The cutting method may also have contributed to this. The end part of the stent was too small for perfect clamping, and the shorter distal part could travel due to the vibrations associated with the cutting process. Additionally, note that Sections 5B and 4A were obtained by inclined cuts with respect to the ascent to the flares, whereupon the silicone could be more stretched and hence deformed in certain parts of the section. We also partly ascribe the instability of the sections to the material loss from the action of the waterjet, which was 1 mm (based on the technological process and machine setting). The differences in the measurements of the two sides of a section, however, are on the order of units percent only, which is insignificant to the primary verification of the results.

Our results also show different thicknesses of silicone on the distal flare part of HV Stent Plus. We believe that the dispersion is due to the specific stent manufacturing process. Regrettably, we were unable to confirm this because of the manufacturer's IP protection.

Testing of the silicone coating and the corrosion resistance of the stent is elaborated in the study (19) focuses on

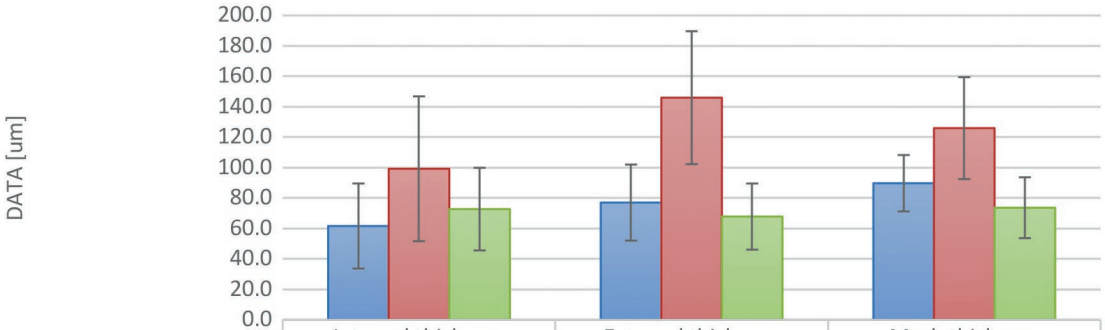

	Internal thickness	External thickness	Mesh thickness
Group I - stent body	61.7	77.1	89.8
Group II - stent flares	99.3	146.0	126.0
Group III - stent terminal	72.8	67.9	73.7

Fig. 5 Comparison of the three monitored thickness parameters: for stent body (Group I), stent flares (Group II) and stent terminal (Group III) with standard deviations. Internal thickness – measurement of the silicone layer on the internal side of the wire. External thickness – silicone thickness on the border of the external side of the wire. Mesh thickness – measurement of the silicone window between the wires.

electrochemical corrosion behavior, which commercial manufacturing companies monitor as undesirable and medically problematic in terms of cracking of uncovered HV Stent Plus. The producer of this stent prepared a set of tests for resistance of silicone against acidic environments to validate the quality of the silicone used. Nine samples of HV Stent Plus were submitted for testing in an acidic environment. The testing solution, which represented an acidic environment in the stomach, was adjusted to pH = 3.0 ± 0.2. The samples were divided into 3 groups of 3 pcs with immersion times of 4, 8, and 12 weeks. The results of the testing showed no significant changes or damage even after 12 weeks of submersion. On one sample, there were few local silicone covering failures present; however, overall stent integrity was not decreased. Based on the results of the above study, we can conclude that the silicone is very stable, and our resin casting method did not chemically affect it for the reported results.

It would be advisable to try to measure the whole stent from the beginning to the end of the same large segments and to determine the size of the silicone layer over the full length of the esophageal HV Stent Plus in more detail. Another option would be to cut the stent longitudinally and compare these data with already measured results. If advisable, future development of the method will compare the observed data with those from a different stent cutting method and use the results to further improve the HV Stent Plus production output inspection process. No suitable data for this are currently available, and this problem will be addressed in the future. This work is timely due to the occurrence of severe patient injury from uncovered stents, when rupture of nitinol reinforcement followed by cavity perforation of a patient occurred in stents produced by Asian manufacturers (20).

CONCLUSION

We developed a simple and reliable method for the evaluation of stent coating quality. In this method, the stent, embedded in a suitable resin, is cut into parts with a waterjet, and the silicone layer is inspected under an optical microscope. The optical method of measuring the silicone layer of the esophageal HV Stent Plus is further improved and can be applied to further procedures and measurements in the future. The quality and sufficient thickness of the silicone layer in the space of the wire crossing were examined, and it was concluded that the silicone layer was strong enough throughout the body stent, flares and terminal part of the stent. By examining the sides of the section, we were able to demonstrate that the data obtained are reasonably consistent and that the cutting process does not affect the properties to the extent of impacting the final measurement results. Evaluation of the different thicknesses in the area of the flares against the stent body falls under the manufacturer's IP and could not be made in detail. The team thus disproved the possible risk of manufacturing defects in the preparation of esophageal HV Stent Plus and confirmed the correctness of the proposed manufacturing and research procedure. This work is a suitable contribution to optimize the design and protection of metallic reinforcements with the help of polymers with the consequent possibility of achieving sufficient homogeneity of the coating and thus validating the process. Overall, the silicone layer thicknesses are consistent with the manufacturing technology used by the manufacturer. Therefore, our measurement validated the manufacturing process and final product quality.

ACKNOWLEDGEMENTS

We would like to thank our laboratory staff and Mrs. Zora Komarkova from the Department of Histology and Embryology of our Faculty for her invaluable help.

This work was supported by the programme PROGRES Q40-09 and programme SVV-260397/2021.

FUNDING

None.

CONFLICT OF INTEREST

The esophageal HV Stent Plus was lent by ELLA-CS, s.r.o., Hradec Kralove, Czech Republic. The authors declare that there is no conflict of interest.

REFERENCES

1. Kozarek R, Baron TH, Song H-Y. Self-expandable stents in the gastrointestinal tract. 1st ed. New York, NY: Springer, 2013: 310.
2. Inbar R, Santo E, Subchi AE-A, et al. Insertion of removable self-expanding metal stents as a treatment for postoperative leaks and perforations of the esophagus and stomach. Isr Med Assoc J 2011; 13: 230–3.
3. Hirdes MMC, Siersema PD, Houben MHMG, Weusten BL a. M, Vleggaar FP. Stent-in-stent technique for removal of embedded esophageal self-expanding metal stents. Am J Gastroenterol 2011; 106: 286–93.
4. Park C-H, Tijing LD, Shon HK, Kim CS. Silicone-coating of nitinol stent wires by electrospinning: catheter deployment test. Dig J Nanomater Biostruct 2014; 9: 1–6.
5. Kim HB, Baik KY, Moon MH, Sung CK. Enhanced corrosion resistance of silicone-coated stents by plasma treatment. Acta Physica Polonica A 2016; 129: 857–60.
6. Talreja JP, Eloubeidi MA, Sauer BG, et al. Fully covered removable nitinol self-expandable metal stents (SEMS) in malignant strictures of the esophagus: a multicenter analysis. Surg Endosc 2012; 26: 1664–9.
7. Hindy P, Hong J, Lam-Tsai Y, Gress F. A Comprehensive review of esophageal stents. Gastroenterology & Hepatology 2012; 8: 526–34.
8. Zhang DS, Dong ZW, Chen B, Yang LZ. Development of CNC lower pressure water jet cutter. Applied Mechanics and Materials 2010; 37: 349–53.
9. Ramulu M, Arola D. Water jet and abrasive water jet cutting of unidirectional graphite/epoxy composite. Composites 1993; 24: 299–308.
10. Li XH, Liao Y, Lei XY, Lu YY, Jiao BQ. Numerically controlled water cutter and its applications in the machining of natural rock materials. Key Engineering Materials 2003; 250: 274–80.
11. Classen M, Tytgat GNJ, Lightdale CJ. Gastroenterological Endoscopy. 2nd ed. New York: Thieme, 2011: 856.
12. Krenács T, Ivnyi B, Bozky B, et al. Postembedding immunoelectron microscopy with immunogold-silver staining (IGSS) in Epon 812, Durcupan ACM and LR-White resin embedded tissues. Journal of Histotechnology 1991; 75–80.
13. Kallivokas SV, Sgouros AP, Theodorou DN. Molecular dynamics simulations of EPON-862/DETDA epoxy networks: structure, topology, elastic constants, and local dynamics. Soft Matter 2019; 15: 721–33.

14. Alberdi A, Suarez A, Artaza T, Escobar-Palafox G, Ridgway K. Composite cutting with abrasive water jet. Procedia Engineering 2013; 63: 421–9.
15. Unde PD, Gayakwad MD, Patil NG, Pawade RS, Thakur DG, Brahmankar PK. Experimental investigations into abrasive waterjet machining of carbon fiber reinforced plastic. Journal of Composites 2015; ID 971596: 1–9.
16. Kong MC, Axinte D, Voice W. Challenges in using waterjet machining of NiTi shape memory alloys: an analysis of controlled-depth milling. Journal of Materials Processing Technology 2011; 211: 959–71.
17. Volenec K, Pohl I. The challenges: stent materials from the perspective of the manufacturer. Gastrointestinal Intervention 2016; 5: 98–104.
18. Quentin T, Poppe A, Bär K, et al. A novel method for processing resin-embedded specimens with metal implants for immunohistochemical labelling. Acta Histochemica 2009; 111: 538–42.
19. Kim Y-S, Kim J-G. Electrochemical corrosion behavior of a non-vascular, bi-stent combination, surgical esophageal nitinol stent in phosphate-buffered saline solution. Mater Sci Eng C Mater Biol Appl 2019; 94: 821–30.
20. Lunt CR, Najaran P, Edwards DE, Bell JK, Mullan D, Laasch H-U. The vanishing stent: repeated fracture and dissolution of nitinol gastric stents in a long term cancer survivor. Gastrointestinal Intervention 2018; 7: 88–90.

Efficacy of Prednisone in Children with Acute Nonspecific Mesenteric Lymphadenitis: A Pilot Study

Momcilo Pavlovic[1,*], Zeljko Rokvic[2], Karolina Berenji[3]

ABSTRACT
Background: Acute nonspecific mesenteric lymphadenitis (ANML) is a common cause of acute abdominal pain in children with no specific treatment. Methods: A total of 13 patients (6 boys, 7 girls) aged 7.3 (5–13.5) years with severe acute abdominal pain were evaluated using ultrasonography and laboratory tests to establish the diagnosis of ANML. They were treated with prednisone 1 mg/kg (max 40 mg daily) for a maximum of 5 days. The intensity of abdominal pain was evaluated before and after treatment using a numeric rating scale. Results: All patients had pain scores above 6/10 before, and below 4/10 after treatment with prednisone. Intensity of abdominal pain after treatment for 1–5 days decreased significantly ($p < 0.001$), with no recurrence at follow-up within 3 months. All other pre-existing signs and symptoms, such as nausea, vomiting, anorexia, fever, diarrhea, and constipation were found to disappear with no adverse effects of corticosteroid therapy. Conclusion: These results suggest that the treatment with prednisone in selective patients with ANML can reduce the duration of abdominal pain.

KEYWORDS
mesenteric lymphadenitis; corticosteroids; abdominal pain; children; lymphoma

AUTHOR AFFILIATIONS
[1] Children's Ambulatory Care Center, Subotica, Serbia
[2] Department of Diagnostic Imaging, General Hospital Subotica, Serbia
[3] Department of Hygiene and Human Ecology, Public Health Institute, Subotica, Serbia
* Corresponding author: Children's Ambulatory Care Center Subotica, Prvomajska 20, 24000 Subotica, Serbia; e-mail: momodec@tippnet.rs

Received: 25 November 2020
Accepted: 22 April 2022
Published online: 29 June 2022

Acta Medica (Hradec Králové) 2022; 65(1): 25–28
https://doi.org/10.14712/18059694.2022.12

INTRODUCTION

Acute nonspecific mesenteric lymphadenitis (ANML) is a well-known and common cause of acute abdominal pain in children. The main symptom of ANML is abdominal pain, often of extreme severity, whereas other characteristic symptoms include fever, diarrhea, constipation, nausea, vomiting, and anorexia accompanied by normal or mild elevated markers of inflammatory conditions (1, 2).

ANML is a self-limiting disease with no specific treatment, and pain disappears within 2–3 weeks (3). The goal of the current pilot study was to evaluate the efficacy of oral prednisone for pain relief in children with ANML.

MATERIAL AND METHODS

A total of 13 children with ANML in the Children's Ambulatory Care Centre were evaluated by the pediatric gastroenterologist (P.M.) between September 2018 and August 2020. Some patients included in this study were reported in detail elsewhere as a case report (4). This study has been performed according to the Declaration of Helsinki and the Research Ethics Board at Children's Ambulatory Care Centre who gave its approval on August 7, 2018 (number 1/08/2018). One of the patient's parents or legal guardian had to sign the consent form before the study inclusion. Only 3 patients with ANML were excluded from the study – one parent refused to sign the consent and another didn't apply the therapy after signing. The third patient was an 8-year-old boy who was not included in the study because the abdominal ultrasound showed thickening of the distal part of the ileum with enlarged, rounded lymph nodes at the mesenteric root scattered throughout the peripheral mesentery. During the examination, abdominal pain was minimal and the patient did not return although further investigations and controls were scheduled. About 23 days after the first occurrence of disturbances, the child's clinical condition worsened with acute onset of colicky pain, rectal bleeding, and signs of ileocolic intussusception. He was hospitalized and after the surgical intervention, histological evaluation of the resected distal segment of ileum and lymph nodes was interpreted as non-Hodgkin's lymphoma (NHL; Burkitt lymphoma subtype).

PRETREATMENT EVALUATION

The diagnosis of ANML in children was made after observing the following conditions: (a) characteristic signs and symptoms; (b) an abdominal ultrasound demonstrating enlarged three or more lymph nodes and short-axis diameter of 8 mm or more in at least one of them; and (c) laboratory and ultrasound exclusion of appendicitis along with other causes of abdominal pain (5). The sonographer used a high-frequency linear transducer (6–13 MHz; Hitachi Medical Corporation, Japan). Ultrasonography performed by an expert sonographer (R.Z.) resulted in the following findings: size criteria of the nodes, the longitudinal diameter and the transverse diameter, and the ratio of the former to the latter calculated to obtain Solbiati index (6).

TREATMENT AND ASSESSMENT OF SYMPTOMS

Patients were treated with a dose of oral prednisone 1 mg/kg (maximum 40 mg) once daily in the morning for 2–5 days. Parents were encouraged to sign consent forms, which stated the use of acetaminophen for analgesia. Patients subjectively evaluated the intensity of the pain using a numeric rating scale (NRS) with numbers ranging from 0 to 10 with 0 denoting "no pain" and 10 representing "worst possible pain" (7). It is notable that we only included patients with pain scores above 6/10 in the study. Pain scores below 4/10 were considered as a satisfactory therapeutic response. The last dose of prednisone was received by patients on the day after the NRS score was found to be below 4/10. There were telephonic reminders for completing the NRS every day, and patients were examined by the pediatric gastroenterologist every 2 days until complete pain relief. All children were encouraged to perform ultrasonography after 1 month. The questionnaire was administered by one of the authors during a clinic visit or a phone interview after 3 months.

The effect of treatment on the intensity of the pain score was analyzed using Chi-square test. In addition, Pearson's correlation test was used to assess the correlation between the reduction of the initial pain and age of patients, duration of pain before treatment, and duration of pain after treatment. Differences were considered to be statistically significant when the p value was 0.05 or less.

RESULTS

Of the 13 patients, 6 were boys and 7 were girls, the mean age of 7.3 ± 2.7 years (age range, 5–13.5 years). All patients except one had other associated symptoms, such as vomiting (7 children), anorexia (5 children), fever (4 children),

Tab. 1 CCharacteristics of 13 patients with acute nonspecific mesenteric lymphadenitis.

Gender (M/F)		7 : 6
Age (y)		7.3 (5–13.5)
Location of pain (n)	Periumbilical	5
	Ileocecal	4
	Ileocecal and periumbilical	4
Time on onset of pain (n)	Daily and noctural pain	9
	Only daily pain	4
Physical examination findings (n)	Ileocecal	5
	Paraumbilical	4
	Diffuse	3
	Epigastric	1
	Rebound tenderness	3
Inflammatory markers (n)	Leukocytosis (≥13.5 × 10^9/L)	0
	C-reactive protein increased (≥5 mg/L)	4

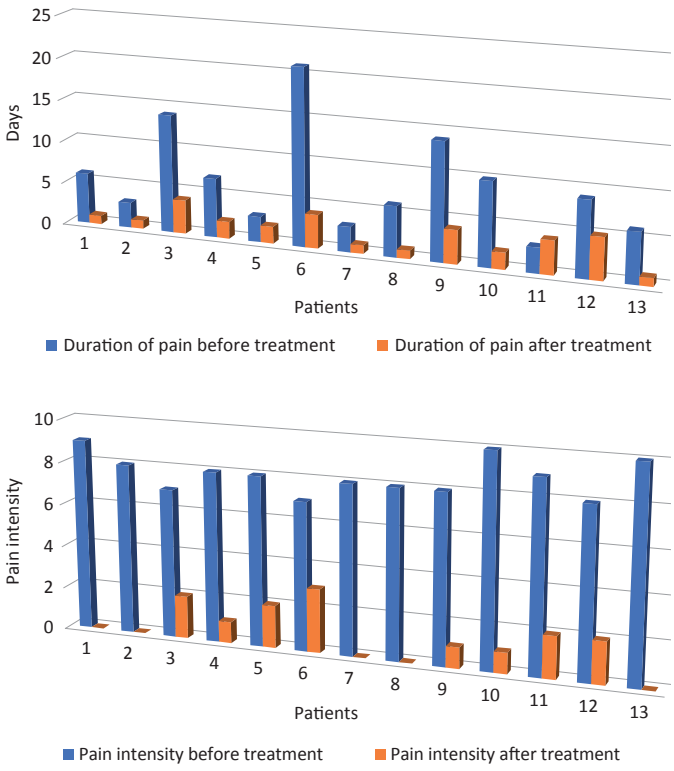

Fig. 1 Pre- and post-treatment duration of pain and pain scores of 13 patients with acute nonspecific mesenteric lymphadenitis.

diarrhea (4 children), and constipation (1 child). One patient described a history of weight loss of 1 kg within 2 weeks. The clinical characteristics, presence of leukocytosis, and increased C-reactive protein are listed in Table 1.

Laboratory tests of the patients included amylase, liver function tests, lactate dehydrogenase (LDH), urea, creatinine, urinalysis and stool parasite analysis were normal in all patients. In 4 patients with diarrhea, the stool culture was negative.

Abdominal ultrasound showed enlarged lymph nodes in all children. Solbiati index was over 2 in all patients, and enlarged lymph nodes were noted only in the mesenterium, with normal dimensions of the spleen and liver. The pre- and post-treatment pain duration, and scores are shown in Figure 1.

In patients with ANML who were treated with prednisone, pain scores decreased significantly at 1–5 days follow-up after the treatment ($X2 = 0.000$; $p < 0.001$). The variable of years with the variable of decrease in initial pain (negative and significant $R = -0.699$, $p = 0.008$) indicates that with the increase of the first, the second variable will fall. The variable of the duration of pain before treatment with the variable of decrease in initial pain (negative and significant $R = -0.588$, $p = 0.035$) indicates that with the increase of the first, the second variable will fall. The variable of duration of pain after treatment with the variable of decrease in initial pain (negative and significant $R = -0.699$, $p = 0.008$) indicates that with the increase of the first, the second variable will fall.

In a 5-year-old girl, the pain disappeared after 3 days and thus the parents ceased the therapy. However, after 1 day without having any disturbances, on the 5th day, the pain intensity increased showing a 7/10 score and we had to continue with prednisone for 2 more days. After that period, the patients' NRS score was 2/10 and we discontinued the use of therapy with no recurrences. In 5 patients, the pain completely disappeared – 3 patients with a pain score of 1, 4 patients had a pain score of 2, and 1 patient had a pain score of 3.

All the other pre-existing signs and symptoms were found to disappear during corticosteroid therapy. A total of 6 patients were examined with control ultrasound 1 month after their inclusion in the study and their mesenterial lymph nodes were normal. After the follow-up period of 3 months, no recurrence of abdominal pain or other gastrointestinal disturbances were noted.

DISCUSSION

Corticosteroids are among the most widely used adjuvant analgesics in the treatment of neuropathic pain, for the management of metastatic bone pain, and also reduce visceral pain (8). The reduction of edema in response to corticosteroid therapy results in the clinical improvement of pain. Additionally, corticosteroids influence the nociceptor activation by decreasing the level of pro-inflammatory cytokines and prostanoids in peripheral neurons, thereby reducing the pathological electrical activity and produce beneficial effects in pain relief (9).

Numerous questions are related to this issue. First, some consider ANML a nondisease that deserves only supportive care (10). However, after the removal of patients' and families' concerns about the illness, they undisputedly expect earlier pain relief so that they can return to normal life. Every day, nocturnal, intensive, long-term pain can be very frustrating and can lead to a negative impact on the patient's quality of life. The alleviation of the pain can be very slow, and symptoms can persist for 3–10 weeks in half of the patients (5). Prednisone might, therefore, present a useful clinical option to meet patients' needs.

Second, many differential diagnoses exist when we encounter patients with mesenteric lymph node enlargement. However, one of the most worrisome diseases for physicians and patients are malignancies, with NHL as the most common primary tumor of the small intestine (11). The effect of pretreatment of corticosteroids on lymphomas has not been fully clarified, but in some patients, they can delay or mask a final diagnosis (12). The terminal ileum is the most commonly reported location of NHL in children younger than 16 years old, because of the high concentration of lymph tissue in that region (13). This is the reason why children with NHL often present with urgent clinical signs of ileocolic intussusception and small bowel obstruction (14), as in our patient who underwent urgent surgical intervention. Otherwise, lymphoma may also present with non-urgent clinical signs as an occult large and single or multiple abdominal masses in the abdomen (15). Ultrasonography and cross-sectional imaging techniques show many characteristic manifestations of NHL, such as the rounded nodes; concurrent involvement of mesenteric, retroperitoneal, and pelvic lymph nodes; and

fusion of enlarged lymph nodes. The NHL mostly involves other abdominal organs, such as the spleen, liver, kidneys, and intestinal tract with circular thickening or dilation of the intestinal cavity (13, 16). Additionally, some laboratory test variables were reported to be useful in predicting malignant diseases. Up-regulation of LDH in malignancies ensures efficient glycolytic metabolism in cancer cells and reduced dependence on oxygen in anaerobic pathway (17). As the tumor's rapid doubling time increases serum LDH, it represents a very valuable enzyme in the evaluation of disease extension (18). Akinci et al. concluded that in adult patients presenting with lymphadenopathy, such results as anemia, leukopenia, thrombocytopenia, high LDH levels, and the presence of splenomegaly, the Solbiati index score below 2 can be used to accurately predict malignant etiology (19). In our patients with ANML, we do not have any of those signs. Although during the diagnostic process a fairly broad list of potential diagnoses can be accurately excluded, and it seems reasonable to repeat sonography after 4–6 weeks.

This pilot study summarizes a subjective experience of pain and is not a placebo-controlled, double-blinded study. However, we believe it was still a valid observation because patients had a fairly good response to the treatment with prednisone and didn't have a recurrence of ANML.

REFERENCES

1. Karmazyn B, Werner EA, Rejaie B, Applegate KE. Mesenteric lymph nodes in children: what is normal? Pediatr Radiol 2005; 35: 774–7.
2. Maconi G. Mesenteric lymphadenopathy. In: Maconi G, Bianchi Porro G, eds. Ultrasound of the gastrointestinal tract. Berlin, Heidelberg: Springer Berlin Heidelberg, 2012: 29–36.
3. Helbling R, Conficconi E, Wyttenbach M, et al. Acute Nonspecific Mesenteric Lymphadenitis: More Than "No Need for Surgery". Biomed Res Int 2017; 2017: 9784565.
4. Pavlovic M, Rokvic Z, Berenji K. Prednisone for the treatment of acute nonspecific mesenteric lymphadenitis. OMJMS 2020; 8: 82–5.
5. Benetti C, Conficconi E, Hamitaga F, et al. Course of acute nonspecific mesenteric lymphadenitis: single-center experience. Eur J Pediatr 2018; 177: 243–6.
6. Solbiati L, Cioffi V, Ballarati E. Ultrasonography of the Neck. Radiol Clin North Am 1992; 30: 941–54.
7. Breivik H, Borchgrevink PC, Allen SM, at al. Assessment of pain. Br J Anaesth 2008; 101: 17–24.
8. Zajączkowska R, Kocot-Kępska M, Leppert W, Wordliczek J. Bone Pain in Cancer Patients: Mechanisms and Current Treatment. Int J Mol Sci 2019; 20: 1451.
9. Mensah-Nyagan AG, Meyer L, Schaefer V, Kibaly C, Patte-Mensah C. Evidence for a key role of steroids in the modulation of pain. Psychoneuroendocrinology 2009; 34: 169–77.
10. Chanchlani R. Clinical profile and management of mesenteric lymphadenitis in children–our experience. Int J Orthopaed, Traumatol Surg Sci 2015; 1: 1–4.
11. Skinner MA, Plumley DA, Grosfeld JL, Rescorla FJ, West KW, Scherer LR. Gastrointestinal tumors in children: an analysis of 39 cases. Ann Surg Oncol 1994; 1: 283–9.
12. Kan E, Levi I, Benharroch D. Alterations in the primary diagnosis of lymphomas pretreated with corticosteroid agents. Leuk Lymphoma 2011; 52: 425–8.
13. Biko DM, Anupindi SA, Hernandez A, Kersun L, Bellah R. Childhood Burkitt Lymphoma: Abdominal and Pelvic Imaging Findings. JR Am J Roentgenol 2009; 192: 1304–15.
14. Ladd AP, Grosfeld JL. Gastrointestinal tumors in children and adolescents. Semin Pediatr Surg. 2006; 15: 37–47.
15. Manzella A, Borba-Filho P, D'Ippolito G, Farias M. Abdominal Manifestations of Lymphoma: Spectrum of Imaging Features. ISRN Radiol 2013; 2013: 483069.
16. Yu RS, Zhang WM, Liu YQ. CT diagnosis of 52 patients with lymphoma in abdominal lymph nodes. World J Gastroenterol 2006; 12: 7869–73.
17. Armstrong AJ, George DJ, Halabi S. Serum lactate dehydrogenase predicts for overall survival benefit in patients with metastatic renal cell carcinoma treated with inhibition of mammalian target of rapamycin. Clin Oncol 2012; 30: 3402–7.
18. Lu R, Jiang M, Chen Z, et al. Lactate dehydrogenase 5 expression in Non-Hodgkin lymphoma is associated with the induced hypoxia regulated protein and poor prognosis. PLoS One 2013; 8(9): e74853.
19. Akinci S, Silay K, Hacibekiroglu T, et al. The predictive value of epidemiological characteristics, clinical and laboratory findings in adult lymphadenopathy etiology. Eur Rev Med Pharmacol Sci 2015; 19: 2973–7.

Progressive Worsening of Snoring as a Rare Presentation of HPV-Positive Oropharyngeal Squamous Cell Carcinoma

V Sha Kri Eh Dam[1], Azliana Aziz[1], Sarah Zulkarnain[2], Nur Asyilla Che Jalil[2], Irfan Mohamad[1,*]

ABSTRACT

The incidence of oropharyngeal squamous cell carcinoma (OPSCC) especially human papillomavirus (HPV) associated type is increasing in trend despite reducing in other head and neck squamous cell carcinoma. Muffled voice, dysphagia, neck mass and pain over the throat are among the common presentations; however, health care professional should be aware of unusual presentation to avoid delay in management. We present a case of HPV-positive OPSCC with a rare presentation; progressive worsening of snoring for 6 months duration. Patient sougth medical attention at the some of private clinics for the past 2 months, however, was told to have a normal tonsillar enlargement. Subsequently, patient was referred to our center with impression of obstructive sleep apnea. We highlight the important of early referral to appropriate center and otorhinolaryngology for assessment in cases presented with worsening snoring.

KEYWORDS

oropharyngeal carcinoma; human papillomavirus; snoring

AUTHOR AFFILIATIONS

[1] Department of Otorhinolaryngology-Head & Neck Surgery, School of Medical Sciences, Universiti Sains Malaysia Health Campus, Kelantan, Malaysia
[2] Department of Pathology, School of Medical Sciences, Universiti Sains Malaysia Health Campus, Kelantan, Malaysia
* Correspondending author: Department of Otorhinolaryngology-Head & Neck Surgery, School of Medical Sciences, Universiti Sains Malaysia Health Campus, 16150 Kota Bharu, Kelantan, Malaysia; e-mail: irfankb@usm.my

Received: 10 December 2020
Accepted: 14 February 2022
Published online: 29 June 2022

Acta Medica (Hradec Králové) 2022; 65(1): 29–32
https://doi.org/10.14712/18059694.2022.13

INTRODUCTION

The incidence of oropharyngeal squamous cell carcinoma (OPSCC) is increasing despite declined in other head and neck squamous cell carcinoma (HNSCC) (1, 2). This is believed due to the gradual decrease in smoking and alcohol intake while increasing in the incidence of human papillomavirus (HPV) infection (1). A 70% of newly diagnosed OPSCCs are HPV positive and HPV was found to be an independent risk factor for OPSCC (3, 4). Interestingly, the majority of HPV-positive head and neck cancers are located in the oropharyngeal region (3).

Patients with oral and oropharyngeal cancer are generally present late at an advanced stage, thus affecting prognosis and survival rate (3, 5). Among the reasons for this are patients considered their conditions as something minor or insignificant and would get better with time (5). The top 3 presenting symptoms are neck mass, sore throat and dysphagia (2, 3). However, these are considered late symptoms as tumour already large enough to cause local pressure to nearby structures, obstructing upper aerodigestive tract and metastasis to the regional lymph node. Patients may have early benign symptoms which not to their concern of the underlying sinister pathology or seek medical attention for other reason and being incidental finding during physical examination. Furthermore, some of the cases may have an atypical presentation which required detail history and examination to reach the diagnosis.

CASE REPORT

A 35-year-old gentleman with no known medical illness, presented with progressive worsening of snoring for the past 6-month duration. He started to seek medical attention 2 months prior because the snoring became louder and disturbed his spouse. It was associated with sleep apnoea, however, no reported daytime somnolence. Besides, his speech also changed as noticed by the friends 2 months ago, however not to patient concern. He denied history of rhinitis symptoms or tonsillitis episodes. Otherwise, there were no history of dysphagia, odynophagia, shortness of breath, sore throat, referred otalgia, bleeding per-oral, neck swelling, loss of appetite, loss of weight, fever and night sweat.

Socially, he works as a teacher, married and blessed with 4 children, non-smoker, non-alcoholic drinker, no high risk behaviour or sexually active, and no family history of malignancy. He visited some of the private clinics for the past 2 months, however, was told to have a normal tonsillar enlargement. He ended up to an otolaryngologist, with the referral of suspecting obstructive sleep apnoea (OSA).

On examination, he was obese with a body mass index of 38 kg/m^2, sitting comfortably without respiratory distress. He had muffled speech, otherwise no stridor or stertor. The oral cavity was normal. Oropharyngeal examination revealed a right tonsillar mass, multi-lobulated surface covered with minimal slough and crossing the midline, with no ulcer or bleeding seen (Figure 1). The left tonsil was grade 1 (according to Friedman et al. grading system (6)) and no restriction of tongue mobility. Other oropharyngeal subsites were hardly visualized, as obscured by the mass. No cervical lymph node or neck mass palpable. Flexible nasopharyngolaryngoscopy revealed a right oropharyngeal mass, crossing the midline and obscuring base of tongue, right vallecula and epiglottis. Otherwise, other laryngeal subsites were normal and no mass seen at bilateral fossa of Rosenmuller.

Biopsy was taken from right oropharyngeal mass, which revealed malignant squamous cell carcinoma, arranged in infiltrative cords and nest with desmoplastic stroma (Figure 2A). The malignant cells are positive for p63 (Figure 2B) and p16 immunohistochemistry staining (Figure 2C). Computed tomography of the base of skull until abdomen was performed and showed large ill-defined heterogeneous enhancing mass measuring 3.5 × 4.5 × 6.5 cm at right oropharyngeal region, occupying the right vallecula and infiltrating right pharyngeal mucosa with no clear

Fig. 1 Oropharyngeal examination shows right oropharyngeal mass (arrow), originated from right tonsil, crossing the midline, multilobulated and covered with minimal slough.

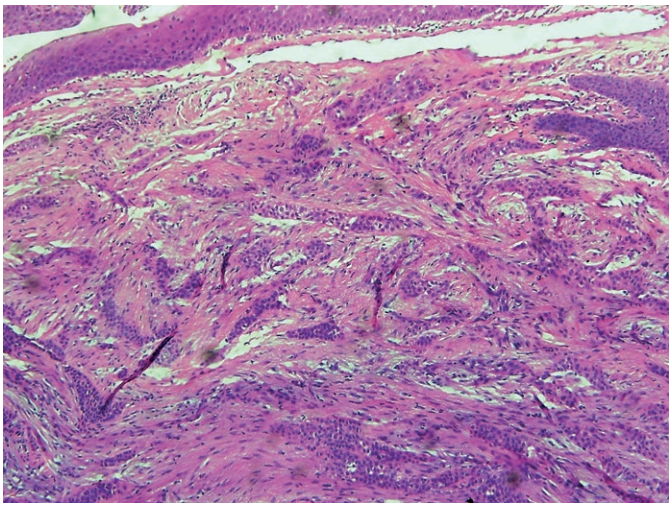

Fig. 2A Haematoxylin & Eosin of Squamous cell carcinoma (100×). Infiltrative tumour arranged in trabeculae and cords with desmoplastic stroma.

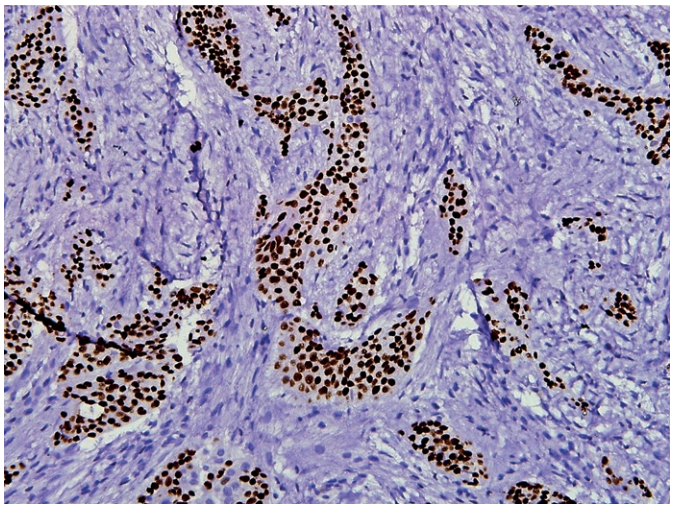

Fig. 2B Immunohistochemical stain (400×). The malignant cells show positive nuclear staining for p63.

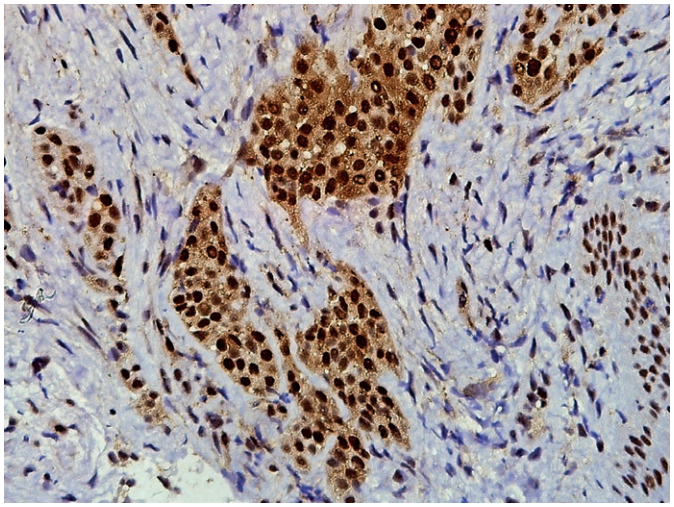

Fig. 2C Immunohistochemical stains (400×). The malignant cells show positive nuclear and cytoplasmic staining for p16.

Fig. 3 Computed tomography, contrasted axial view at level of oropharynx shows large ill-defined heterogenous enhancing mass measuring 3.5 × 4.5 × 6.5 cm at oropharynx region, occupying the right vallecula and infiltrating right pharyngeal mucosa with no clear fat plane with base of tongue and epiglottis.

fat plane with the base of tongue and epiglottis (Figure 3). Also, multiple cervical lymph nodes enlargement was seen including bilateral level Ib and IIa, right level IIb and left level III (largest at left level IIa measuring 0.8 cm × 1.7 cm). No distant metastasis visualised from the scan, thus his staging was $T_3N_2M_0$ (according to latest TNM staging, 8th edition, by American Joint Committee on Cancer (7)).

A multidiscipline team meeting was conducted with a consensus that the patient would be more beneficial from chemoradiotherapy (CRT). Patient was explained regarding the modality of treatments either surgery or CRT, and he opted for CRT.

DISCUSSION

Demographic profiles, risk factors and tumour characteristics are different between HPV-positive and HPV-negative OPSCCs (2, 3). HPV-related OPSCC is currently considered a distinct disease due to its specific characteristic and oncogenic HPV aetiology (8). High-risk HPV infection of oropharynx will produce two crucial viral oncoproteins; E6 and E7. These oncogenes can inactivate p53 and pRB tumour suppressor gene, which lead to dysregulation of the cell cycle. Inactivation of pRB by viral oncoprotein E7 will result in overproduction of p16. High-level of p16 expression is an excellent marker for high-risk HPV-related cancers. Therefore, p16 immunohistochemistry is used as a surrogate marker for HPV-positive OPSCC (9).

Most of HPV-positive OPSCC patients are found to be younger, white males, non-smoker, generally healthier, sexually active and higher socio-economical group, while patients are generally older with history of heavy smoking and alcohol consumption in HPV-negative OPSCC (2, 3). Furthermore, HPV-positive OPSCC is found more common in a western country and believed due to changing in sexual practices with increasing in oral sexual behaviour (10). The prevalence of HPV-positive OPSCC was found to be dramatically increased for the last two decades, from 40.5% before 2000, to 64.3% between 2000 and 2004, 72.2% between 2005 and 2009 and 81% between 2008 to 2013 (2, 11). These features not only simply explained the disease is increasing in trend, it also implies more people will be diagnosed with malignancy at a younger age.

Although prognosis is relatively better than HPV-negative OPSCC, generally patient presented late which usually require multimodality of treatments (2). Apart from the advanced disease itself, a combination of surgery, radiotherapy and/ or chemotherapy will result in higher morbidity. Thus, early presentation and detection of the

disease are the main key factor for a better outcome in term of prognosis and survival rate. Several studies conducted to identify the initial symptoms OPSCC, and generally concluded that neck mass is the commonest presentation of HPV-positive OPSCC while sore throat or pain is more common in HPV-negative OPSCC (2,3). Other less common presentations are dysphagia, globus sensation, direct visualisation and otalgia (2, 12).

Health care professional especially at primary care should be aware that there is a small percentage of patient who is asymptomatic and only incidental finding during medical check-up (2, 11). Studies have shown that most of the patients remained asymptomatic if tumour smaller than 2cm or still at T1 stage (5, 13). Early detection and referral to the appropriate centre is very important as there is a positive association between delay in referral, the advanced stage during initial presentation, and poor survival (12).

Our patient was initially referred from the primary care centre for suspecting obstructive OSA secondary to tonsillar hypertrophy, as he was considered as a low-risk group for malignancy. Although the patient is obese, progressive worsening of snoring without recent markedly increase in weight, frequent rhinitis symptoms or recurrent tonsillitis warrant thorough examinations or early referral to otorhinolaryngology to look for other pathology apart from OSA. In addition, associated changes of voice should denote something more sinister underlying pathology. Furthermore, malignancy should be suspected in unilateral tonsil enlargement, especially with the present of cervical lymph node enlargement. A 20% of patient with asymmetry tonsillar enlargement were found to have malignancy, either lymphoma or squamous cell carcinoma (14). Characteristic of tonsil on examination is also important to differentiate between benign and malignant. Presence of irregular surface, ulcer or bleeding usually suggested of malignancy. Due to its special characteristics compared to other types of HNSCC, HPV-positive OPSCC should be suspected in traditionally considered low-risk patients like younger age and non-smoker. The unusual presentations in our case are the main reason for the delay in referral.

Some of the head and neck tumors like lymphoma, sarcoma, pleomorphic adenoma, mycosis fungoides, paraganglioma, and rhabdomyoma have been reported to present with OSA symptoms (15). The worsening of upper airway obstruction which is the hallmark of OSA could be contributed by the disruption of the normal anatomy or physiology of upper airway by the tumors (15, 16). Anatomically, progressive enlarging of the tumors result in progressive narrowing of the upper airway or pharyngeal space. On the other hand, head and neck tumor also may result in cranial nerves palsy especially glossopharyngeal and vagus nerves. Loss of these nerves function significantly resulting in weakness of pharyngeal dilator muscles and further narrow the upper airway. OPSCC as seen in the present case is a good example of anatomical factor, while in the more advance cases of OPSCC, neural factor also may involved.

Management of HPV-positive OPSCC is depend on the stage of the disease. Due to its distinct entity, the latest American Joint Committee on Cancer, 8th edition has revised on TNM staging of OPSCC by dividing it into HPV-associated and non-HPV-associated (7). Early-stage usually require single-modality treatment either surgery or radiation, whereas late-stage carcinomas normally require multimodality treatment with combinations of surgery, radiation, and/or chemotherapy (2).

CONCLUSION

Worsening of snoring could be the only symptom of HPV-positive OPSCC as the result of progessive enlargement of the tumor and narrowing of the upper airway. The health care professional should be aware of this unusual presentation and early referral to otorhinolaryngology is vital.

REFERENCES

1. Elrefaey S, Massaro MA, Chiocca S, Chiesa F, Ansarin M. HPV in oropharyngeal cancer: the basics to know in clinical practice. Acta Otorhinolaryngol Ital 2014; 34(5): 299–309.
2. McIlwain WR, Sood AJ, Nguyen SA, Day TA. Initial symptoms in patients with HPV-positive and HPV-negative oropharyngeal cancer. JAMA Otolaryngol Head Neck Surg 2014; 140(5): 441–7.
3. Carpén T, Sjöblom A, Lundberg M, et al. Presenting symptoms and clinical findings in HPV-positive and HPV-negative oropharyngeal cancer patients [published correction appears in Acta Otolaryngol 2018 Jul; 138(7): 675]. Acta Otolaryngol 2018; 138(5): 513–8.
4. You EL, Henry M, Zeitouni AG. Human papillomavirus-associated oropharyngeal cancer: review of current evidence and management. Curr Oncol 2019; 26(2): 119–23.
5. Rogers SN, Vedpathak SV, Lowe D. Reasons for delayed presentation in oral and oropharyngeal cancer: the patients' perspective. Br J Oral Maxillofac Surg 2011; 49(5): 349–53.
6. Friedman M, Salapatas AM, Bonzelaar LB. Updated Friedman staging system for obstructive sleep apnea. Adv Otorhinolaryngol 2017; 80: 41–8.
7. Kato MG, Baek CH, Chaturvedi P, et al. Update on oral and oropharyngeal cancer staging - International perspectives. World J Otorhinolaryngol Head Neck Surg 2020; 6(1): 66–75.
8. De Felice F, Tombolini V, Valentini V, et al. Advances in the Management of HPV-Related Oropharyngeal Cancer. J Oncol 2019; 2019: 9173729. Published 2019 Apr 14.
9. Sedghizadeh PP, Billington WD, Paxton D, Ebeed R, Mahabady S, Clark GT, Enciso R. Is p16-positive oropharyngeal squamous cell carcinoma associated with favorable prognosis? A systematic review and meta-analysis. Oral Oncology 2016 Mar 1; 54: 15–27.
10. Stein AP, Saha S, Kraninger JL, et al. Prevalence of Human Papillomavirus in Oropharyngeal Cancer: A Systematic Review. Cancer J 2015; 21(3): 138–46.
11. Mehanna H, Beech T, Nicholson T, et al. Prevalence of human papillomavirus in oropharyngeal and nonoropharyngeal head and neck cancer – systematic review and meta-analysis of trends by time and region. Head Neck 2013; 35(5): 747–55.
12. Pitchers M, Martin C. Delay in referral of oropharyngeal squamous cell carcinoma to secondary care correlates with a more advanced stage at presentation, and is associated with poorer survival. Br J Cancer 2006; 94(7): 955–8.
13. Mashberg A, Meyers H. Anatomical site and size of 222 early asymptomatic oral squamous cell carcinomas: a continuing prospective study of oral cancer. II. Cancer 1976; 37(5): 2149–57.
14. Tobias Gómez S, Palomar Asenjo V, Borràs Perera M, Pérez Hernández I, Ruiz Giner A, Palomar García V. Significación clínica de la asimetría amigdalina [Clinical significance of unilateral tonsillar enlargement]. Acta Otorrinolaringol Esp 2009; 60(3): 194–8.
15. Faiz SA, Balachandran D, Hessel AC, et al. Sleep-related breathing disorders in patients with tumors in the head and neck region. Oncologist 2014; 19(11): 1200–6.
16. Friedman M, Landsberg R, Pryor S, Syed Z, Ibrahim H, Caldarelli DD. The occurrence of sleep-disordered breathing among patients with head and neck cancer. Laryngoscope 2001; 111(11 Pt 1): 1917–9.

Bilateral Mature Ovarian Teratoma with Torsion in a Premenarchal Girl

Jana Lešková[1,*], Jaroslav Thierry Kříž[2], Radek Štichhauer[1]

ABSTRACT

Mature cystic teratoma is the most common type of ovarian tumor in children. Adnexal torsion is the main complication of mature ovarian teratoma. The synchronous bilateral incidence of mature cystic teratoma in premenarchal girls is known to be rare. However, the incidence of adnexal torsion is higher in young girls. A 10-year-old girl presenting with acute abdomen was managed by emergency laparotomy. Bilateral mature ovarian teratoma with adnexal torsion of the right ovary was found. The right ovarian tissue was not viable due to torsion and an oophorectomy was necessary. Cystectomy with preservation of the ovarian tissue of the left ovary was performed. Histopathological diagnosis was bilateral synchronous mature teratoma with necrosis of the right adnexa. Although the risk of malignancy of torsed ovaries and mature teratomas in premenarchal girls is low, their removal is recommended to prevent adnexal torsion. Decision between ovarian tissue sparing surgery or oophorectomy depends on the risk of malignancy, fertility preservation and the avoidance of early menopause.

KEYWORDS

premenarchal girl; adnexal torsion; ovarian teratoma; surgery

AUTHOR AFFILIATIONS

[1] Department of Pediatric Surgery and Traumatology, Charles University, Faculty of Medicine and University Hospital, Hradec Králové, Czech Republic

[2] Department of Obstetrics and Gynecology, Charles University, Faculty of Medicine and University Hospital, Hradec Králové, Czech Republic

* Corresponding author: Department of Pediatric Surgery and Traumatology, Charles University, Faculty of Medicine and University Hospital, Hradec Králové, Czech Republic; e-mail: jana.leskova@fnhk.cz

Received: 27 January 2021
Accepted: 5 April 2022
Published online: 29 June 2022

Acta Medica (Hradec Králové) 2022; 65(1): 33–36
https://doi.org/10.14712/18059694.2022.14

INTRODUCTION

Ovarian tumors are rare, comprising only 1.5% of all childhood tumors (1). Within the group of ovarian tumors, ovarian teratomas are the most common type of ovarian germ cell tumors in children and account for 27% of all teratomas in large series. Teratomas are classified as mature, immature and malignant (2). The most common ovarian tumors in children are mature cystic teratomas, consisting up to 20% of all the ovarian tumors (1). The bilateral presence is in 12% of all cases and risk of malignancy is approximately 2% (3). Adnexal torsion is a rare pediatric surgery emergency, but is the main complication of mature ovarian teratomas (4). In the case report is presented a case of bilateral synchronous mature ovarian teratomas with torsion in a premenarchal girl, which was managed in our department.

CASE REPORT

A 10-year-old previously healthy girl was admitted to the hospital, as emergency due to abdominal pain, nausea and repeated vomiting. The patient presented with a complaint of intermittent lower abdominal pain for two days that worsened over last 12 hours. On physical examination a palpable firm mass was identified and distension of the abdomen was observed. The ultrasound scan revealed mass of cystic-solid composition without calcification and other three cystic masses in the pelvic region. The size of the largest structure was found to be 10 cm in diameter. The chest X-ray was performed with normal findings. CT or MRI scan was not done because of emergency. Serum tumor and inflammatory markers were within the normal range. Under a diagnosis of acute abdomen with lower abdominal tumor, the patient was indicated to the laparotomy. The patient was operated on 3 hours after admission to the hospital. Preoperative diagnosis was suspected as an ovarian tumor with adnexal torsion. The initial operative finding revealed a torsion of the right ovary. The average right ovary size was found to be 9 cm in diameter. Right ovarian tissue was completely twisted 720 degrees (Fig. 1). The ovary was not salvaged with detorsion because of its necrosis. Due to irreversible ischemic damage of the ovary, right oophorectomy was necessary (Fig. 2). Under next observation the other cystic mass on the left ovary was noted with an average size of 6 cm in diameter (Fig. 3). Cystectomy with preservation of the ovarian tissue of the left ovary was performed (Fig. 4). Histopathological examination showed bilateral synchronous mature teratoma with necrosis of the right adnexa. The postoperative course was uneventfull and the patient was discharged on the 5th day after surgery.

DISCUSSION

Teratomas are the most common histologic subtype of childhood ovarian germ cell tumors (2). Their optimal operative management in this age group still remains unclear because of the rarity of such tumors and depends on retrospective studies (1, 5). In scoping review from Poland authors have revealed a number of knowledge gaps in the

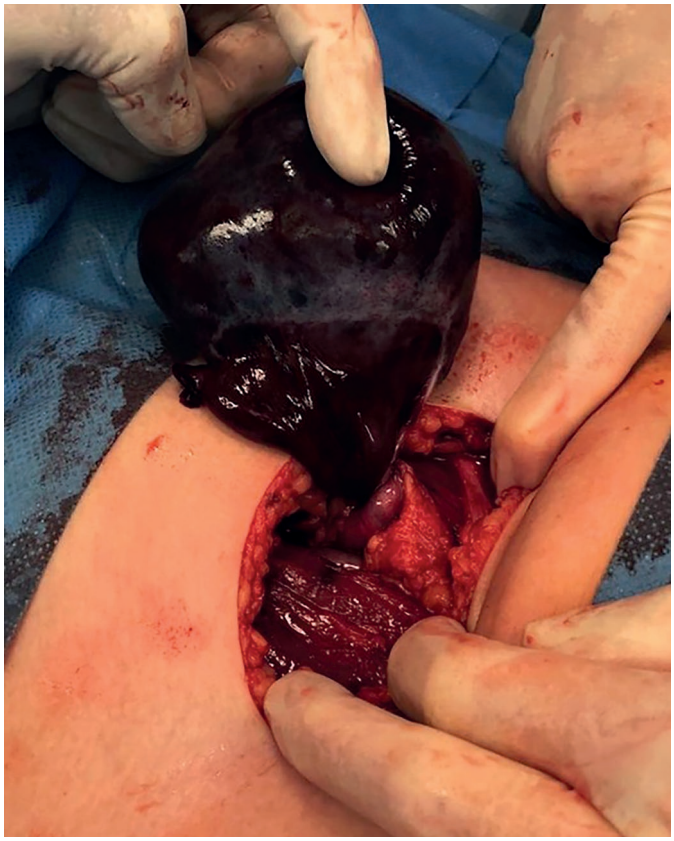

Fig. 1 The torsion of the right ovary. The right ovary size was 9 cm in diameter and ovarian tissue was completely twisted 720 degrees.

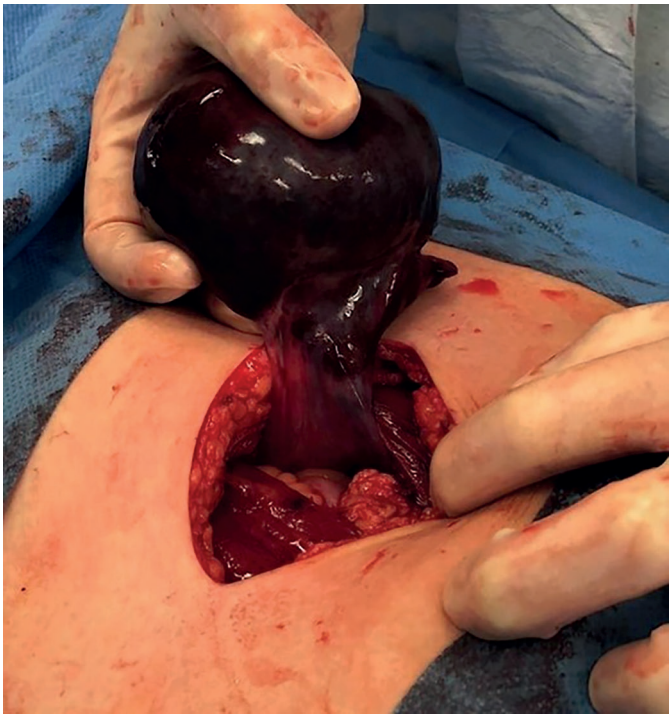

Fig. 2 The right ovary after detorsion. Due to irreversible ischemic damage to the ovary, right oophorectomy was necessary.

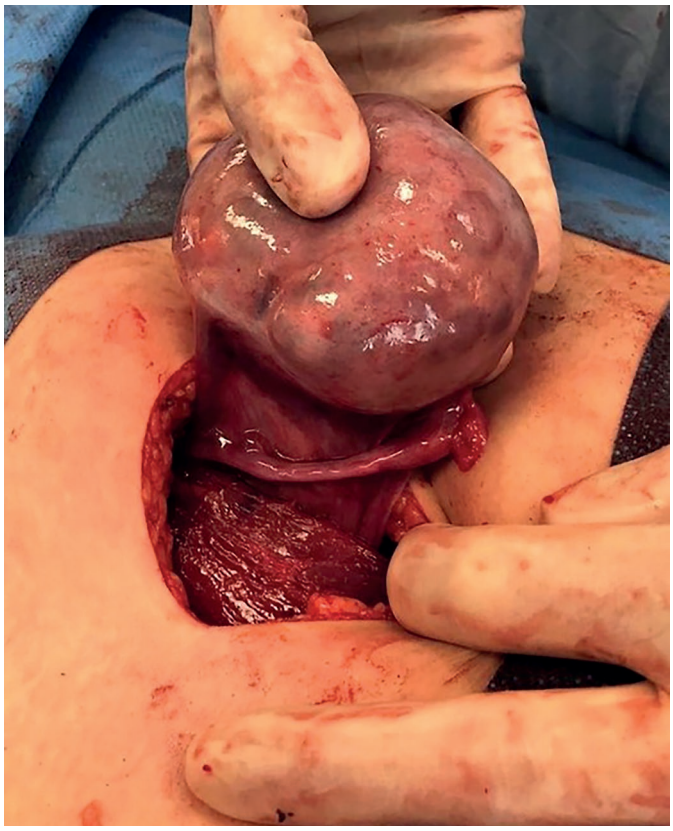

Fig. 3 The cystic mature teratoma of the left ovary. The average size was 6 cm in diameter. Cystectomy with preservation of the ovarian tissue of the left ovary was performed.

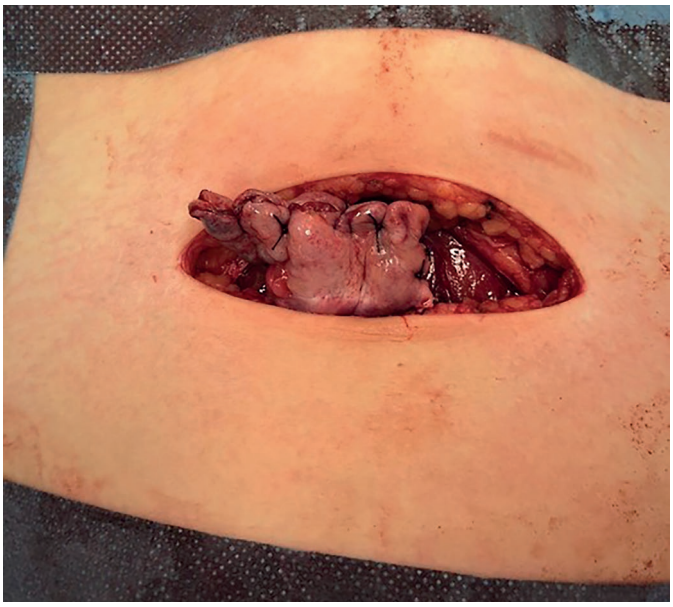

Fig. 4 Finished suture of the rest of the left ovarian tissue after cystectomy.

evidence based medicine for pediatric ovarian teratomas (6). The other systematic review reported by Renaud et al. also has revealed lack of prospective and randomized trials (1).

We present rare case of bilateral synchronous mature ovarian teratomas with torsion in a premenarchal girl, which was managed in our depatrment. The first case was reported by authors from Japan in 2006 (7). Although mature cystic teratomas are the most common ovarian tumors in children (2), their unilateral incidence is known to be rare in premenarchal girls and synchronous bilateral incidence is even more unusual. Mature teratomas are bilateral in only 12% of cases and become malignant in approximately 2% (3). Although the overall rate of malignancy in torsed ovaries is low and mature teratomas in premenarchal girls are rarely malignant, their removal may be performed to prevent adnexal torsion (1, 4). Adnexal torsion is the main complication of mature ovarian teratomas (4, 8) and the incidence of adnexal torsion is associated with younger age (4, 9). Decision between ovarian tissue sparing surgery or oophorectomy dependents on the risk of malignancy, fertility preservation and the avoidance of early menopause.

In a nationwide population-based cohort study from the Netherlands there was an exponential increase of the adnexal masses in relation with age. The proportion of malignancy in this study was highest in the premenarchal girls. Oophorectomies were more often performed in the premenarchal age group, while ovarian sparing surgeries were more common in postmenarchal patients both in benign mass (10). Presumption of malignancy and necrosis caused by torsion may necessitate oophorectomy (9). The treatment of the torsion is an emergency and must be as conservative as possible in order to preserve the ovarian function. Oophorectomy is reserved for necrotic ovaries. The toreable duration for functional preservation of ovarian tissue after adnexal torsion in premenarchal girls has not been established yet. Report from Takeda et al. suggested that preservation of ovarian tissue was possible if surgery was performed within 8 hours after symptom onset (7). In our report it was more than 12 hours after symptom onset and oophorectomy was necessary because of irreversible ischemic damage of ovarian tissue. This ischemic damage was dependant on the degree of torsion too. The current literature suggests that it is safe to perform only detorsion, regardless of the level of ischemia or volume of the torsed ovary (11). In our case right ovary could not be salvaged with detorsion as the tissue was completely necrotic and did not recover despite detorsion. As in other reports (4, 12), cystectomy was performed in our patient on the left ovary. Ovarian tissue sparing technique with preservation of the ovarian tissue of the affected gonad in children should be successfully applied as much as possible, considering normal puberty, future fertility and the lower incidence of malignancy in this age group (4, 9). However, inadequate resection or staging in the setting of a malignancy may place the patient at risk for unnecessary adjuvant therapy or recurrent disease. The premenarchal girl in our case had bilateral synchronous mature ovarian teratomas with torsion of the right ovary. Elective oophoropexy was not performed because of the fear that residue of the left ovarian tissue may be negatively influenced by pexy sutures in the future. Oophoropexy should decrease the risk of subsequent contralateral torsion but there is no evidence showing its efficacy in pediatric age group. The role of oophoropexy in treating ovarian torsion is still not clear (2, 9, 11).

An other important aspect of the management of ovarian teratomas is their recurrence rate and the incidence of bilateral lesions. In the UK nationwide study recurrence occurred in 4.8%, 2.9% children had synchronous tumors and 3.2% were diagnosed with metachronous tumors (13). The authors demonstrated that ovarian tumor recurrence and metachronous disease occur, even in tumors that were previously deemed as benign lesions (13). All pediatric patients should undergo follow-up surveillance after resection of an ovarian tumor including benign lesions to ensure the early detection of metachronous contralateral lesions or ipsilateral recurrence. The unilateral oophorectomy for ovarian tumors reduces the risk of tumor recurrence, but it may have negative effects on later oocyte production and may result in earlier menopause (1). Chabaud-Williamson et al. evaluated in their retrospective study endocrine function and fertility after unilateral oophorectomy that was performed for the first tumor in patients who were initially treated for unilateral ovarian teratoma but were subsequently diagnosed with a contralateral lesion. The patients had regular normal menstruations and the eldest had a spontaneous and normal pregnancy at last follow-up (14). Thus, patients who are managed by unilateral oophorectomy for ovarian teratoma may have regular menstruations and spontaneous pregnancies.

CONCLUSION

Mature teratomas are generally diagnosed in reproductive age group. Unilateral incidence is known to be rare in premenarchal girls, synchronous bilateral is even more unusual. However, the incidence of adnexal torsion is higher in young girls. Although the overall rate of malignancy in torsed ovaries is low and mature teratomas in premenarchal girls are rarely malignant, their removal may be performed to prevent adnexal torsion. Decision between ovarian tissue sparing surgery and oophorectomy depends on the risk of malignancy, fertility preservation and the avoidance of early menopause. All pediatric patients should undergo follow-up surveillance after resection of an ovarian tumor including benign lesions to ensure the early detection of metachronous contralateral lesions or ipsilateral recurrence.

REFERENCES

1. Renaud EJ, Sømme S, Islam S, et al. Ovarian masses in the child and adolescent: An American Pediatric Surgical Association Outcomes and Evidence-Based Practise Committee systematic review. J Pediatr Surg 2019;54:369-377.
2. Holcomb GW, Murphy JP, Ostlie DJ. Ashcrafts pediatric surgery. 6th ed. Elsevier Sunders, 2014: 935–8, 1051–5.
3. Symonds EM, Symonds IM. Essential Obstetrics and Gynaecology. 4th ed. Elsevier Science, 2004: 324–34.
4. Rabinovich I, Pekar-Zlotin M, Bliman-Tal Y, Melcer Y, Vaknin Z, Smorgick N. Dermoid cysts causing adnexal torsion: What are the risk factors? Eur J Obstet Gynecol Reprod Biol 2020; 251: 20–2.
5. Takayasu H, Masumoto K, Tanaka N, et al. A clinical review of ovarian tumors in children and adolescents. Pediatr Surg Inter 2020; 36: 701–9.
6. Łuczak J, Bagłaj M, and Dryjański P. What recent primary studies tell us about ovarian teratomas in children: a scoping review. Cancer Metastasis Rev 2020; 39(1): 321–9.
7. Takeda A, Manabe S, Mitsui T and Nakamura H. Laparoscopic Management of Mature Cystic Teratoma of Bilateral Ovaries with Adnexal Torsion Occurring in a 9-Year-Old Premenarchal Girl. J Pediatr Adolesc Gynecol 2006; 19: 403–6.
8. Fayez I, Khreisat B, Athamneh T, Omoosh R, and Daibes MA. Multiple Bilateral Ovarian Mature Cystic Teratomas with Ovarian Torsion: A Case Report. Oman Med J 2018; 33(No. 2): 163–66.
9. User IR, Karakuş SC, Özokutan BH, Akçaer V, Burulday B, Ceylan H. Can preoperative findings help to interpret neplastic and non-neoplastic lesions of ovary and affect surgical decisions in children and adolescents? Arch Argent Pediatr 2019; 117(5): 294–300.
10. Hermans AJ, Kluivers KB, Janssen LM, et al. Adnexal masses in children, adolescents and women of reproductive age in the Netherlands: A nationwide population-based cohort study. Gynecologic Oncology 2016; 143: 93–7.
11. Geimanaite L, Trainavicius K. Pediatric ovarian torsion: Follow-up after preservation of ovarian tissue. J Pediatr Surg 2019; 54: 1453–6.
12. Cribb B, Vishwanath N, Upadhyay V. Paediatric ovarian lesions – the experience at Starship Children's Hospital, New Zealand. NZMJ 2014; 127(No 1395).
13. Braungart S, CCLG Surgeons Collaborators, Craigie RJ, Farrelly P, Losty PD. Ovarian tumors in children: how common are lesions recurrence and metachronous disease? A UK CCLG Surgeons Cancer Group nationwide study. J Pediatr Surg 2020; 55: 2026–9.
14. Chabaud-Williamson M, Netchine I, Fasola S, et al. Ovarian-Sparing Surgery for Ovarian Teratoma in Children. Pediatr Blood Cancer 2011; 57: 429–34.

Rapidly Progressive Interstitial Lung Disease Associated with Melanoma Differentiation-Associated Gene 5 Antibody

Yosuke Maezawa[1], Mami Narita[1], Riho Tanimura[1], Sou Hattori[1], Hiroaki Satoh[2,*]

ABSTRACT

Anti-melanoma differentiation-associated gene-5 (MDA-5) antibody is an autoantibody found in patients with dermatomyositis. These antibody-positive patients are clinically characterized by complications of rapidly progressive interstitial pneumonia resistant to treatment and with poor prognosis. We describe herein a patient with MDA-5 antibody-positive interstitial lung disease, which progressed rapidly to death after a period of slow progress. Recently, attention has been paid to the similarities in clinical courses and CT images between MDA-5 antibody-positive interstitial lung disease and coronavirus disease 2019 (COVID-19)-associated pneumonia. Patients with MDA-5 antibody do not always have diffuse and evenly distributed bilateral opacities at the time of first presentation. This patient had significant laterality of such opacities. It should be considered that MDA-5 antibody-positive patients with such laterality in opacities might progress rapidly. Chest physicians, dermatologists, and dermatologists need to be aware of the characteristics of the disease for optimal treatment choices.

KEYWORDS

interstitial lung disease; anti-melanoma differentiation-associated gene-5 antibody: smoking; prognosis

AUTHOR AFFILIATIONS

[1] Division of General Medicine, University of Tsukuba, Mito Medical Center-Mito Kyodo General Hospital, Mito, Ibaraki, Japan
[2] Division of Respiratory Medicine, University of Tsukuba, Mito Medical Center-Mito Kyodo General Hospital, Mito, Ibaraki, Japan
* Corresponding author: Division of Respiratory Medicine, Mito Medical Center, University of Tsukuba-Mito Kyodo General Hospital, Miya-machi 3-2-7, Mito-city, Ibaraki, 310-0015, Japan; e-mail: hirosato@md.tsukuba.ac.jp

Received: 21 June 2021
Accepted: 26 April 2022
Published online: 29 June 2022

Acta Medica (Hradec Králové) 2022; 65(1): 37–40
https://doi.org/10.14712/18059694.2022.15

INTRODUCTION

Anti-melanoma differentiation-associated gene-5 (MDA-5) antibody is an autoantibody found in patients with dermatomyositis, especially those with typical skin findings but no myositis (1). These antibody-positive patients are clinically characterized by complications of rapidly progressive interstitial lung disease (ILD) resistant to treatment and with poor prognosis (1). MDA-5 is a protein molecule belonging to the retinoic acid-inducible gene-I (RIG-I) family. RIG-I family proteins contribute to protection from viral infection (2). Therefore, MAD-5 is involved not only in the development of dermatomyositis but also plays an important role in antiviral immunity (2). Recently, attention has been paid to the similarities in clinical courses (3, 4) as well as in CT images (5–10) between MDA-5 antibody-positive ILD and coronavirus disease 2019 (COVID-19)-associated pneumonia. Bilateral subpleural ground glass-like opacities (GGOs) spreading in the lower lobe were the most common findings (5–10).

We describe herein a patient with MDA-5 antibody-positive ILD, which progressed rapidly to death. The patient had unilateral non-diffuse opacities at the time of the first visit, and worsened rapidly to die shortly thereafter.

CASE REPORT

A 77-year-old man presented after having experienced two weeks of general fatigue and dyspnea. The patient reported having had spinal stenosis five years prior and was followed up by orthopedic outpatient clinic in our hospital. A chest radiograph ten months before this consult showed no reticular opacities in the left lower lung field (Figure 1). He was a 15 pack-year past ex-smoker. On admission, he was alert. His vital signs were: blood pressure of 122/64 mmHg, pulse rate of 69/min, and body temperature of 38.0 °C. Percutaneous arterial blood oxygen saturation was 98% in room air. Pharyngeal redness and hoarseness were observed. Fine crackles at the lung base were not observed. Superficial lymph node swelling was not observed, neither were Gottron signs, swelling, heliotrope rash, purpura, arthritis, or other physical findings suggestive of dermatomyositis. Muscle weakness was also not apparent. On admission, his white blood cell count was 5600/μL, and C-reactive protein was 6.12 mg/dL. Creatine kinase was 154 IU/L, lactic dehydrogenase was 446 U/L, and ferritin was 2469.3 ng/mL; β-D glucan was below 5.0pg/mL. Chest computed tomography (CT) scan revealed peripheral GGOs and consolidation, consistent with MDA-5 antibody-positive ILD (7, 8) (Figure 2, Table 1). These changes were more pronounced in the right lung than in the left lung (Figure 2). Considering his respiratory condition, reverse transcription-polymerase chain reaction (RT-PCR) for COVID-19 was performed, but the result was negative. The patient was initially diagnosed with community-acquired pneumonia, and was subsequently started on antibiotic treatment with tazobactam/piperacillin, but his symptoms of dyspnea and weakness did not improve. On admission, the patient tested negative for autoantibodies against anti-aminoacyl tRNA synthetase (ARS), cyclic citrullinated peptide antibody (CCP), antinuclear antibody (ANA), as well as anti-neutrophil cytoplasmic autoantibodies against proteinase 3 (PR3-ANCAs), and myeloperoxidase (MPO-ANCAs). MDA5 antibody had a high titer index >150 (normal range, 0–32). The patient's condition worsened nine days after admission and 10 L/min oxygen was required. A chest CT scan revealed exacerbation of the ground-glass opacities in the right lower lung, but not evenly on both sides (Figure 3). The patient was transported to the ICU and placed on respiratory support because of worsening oxygenation. The high level of ferritin, rapidly progressive respiratory failure, and findings on chest CT suggested the possibility of rapidly progressive ILD. Methylprednisolone (1000 mg/day, drip infusion) was administered for acute respiratory failure for three days and was continued at a reduced dose (500 mg/day) without improvement. Therefore, cyclophosphamide (500 mg, drip infusion) and tacrolimus (4 mg once daily for ten days) were added to the steroid regimen. The patient's condition did not improve, and he died of respiratory failure on day 10 after admission.

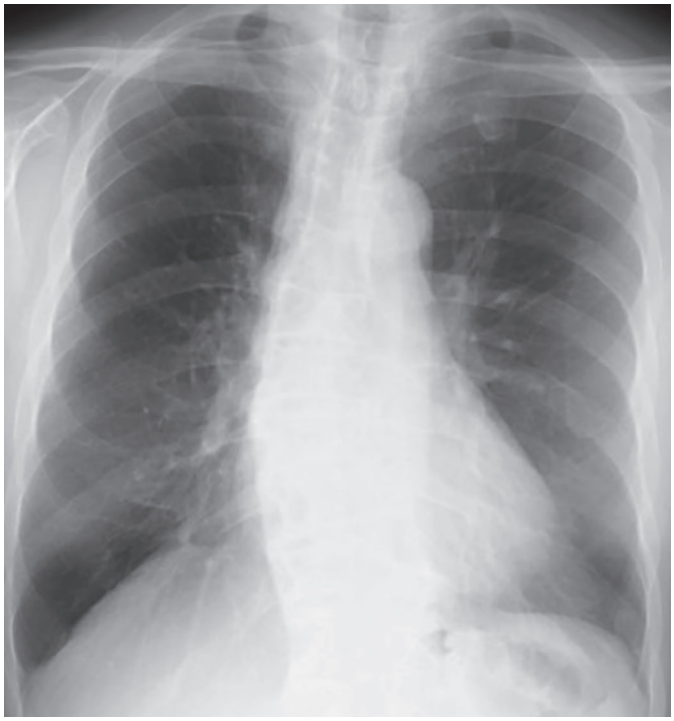

Fig. 1 A chest radiograph 10 months before the patient's presentation showed no reticular opacities in the left lower lung field.

DISCUSSION

Two previous studies have described the characteristics of CT images of MDA-5 antibody-positive ILD (7, 8). A study by Tanizawa et al. pointed out the importance of the following three findings: lower peripheral or peribronchovascular consolidations or GGO, lower peripheral or peribronchovascular reticulation, and random peripheral GGO (7). Another study by Chino et al. described the importance of perilobular opacities, which thickened and consolidated

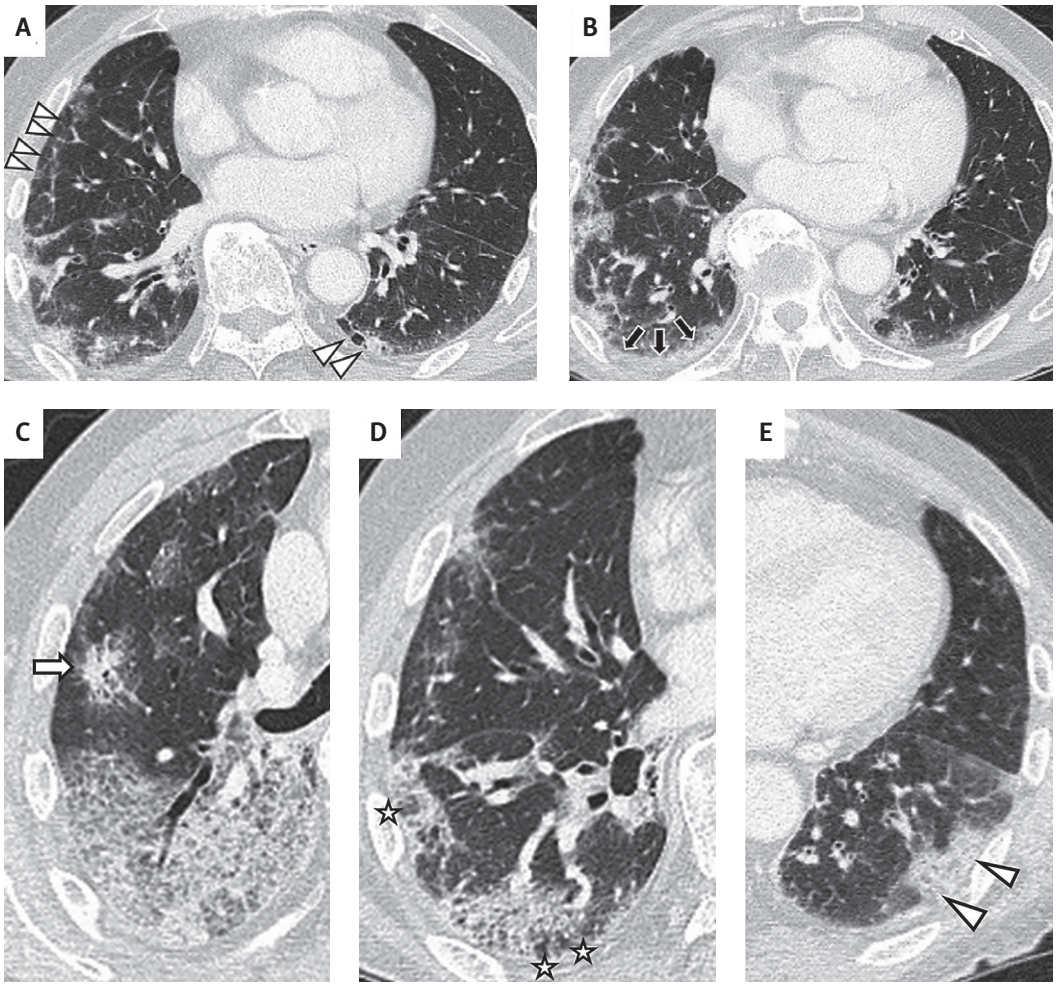

Fig. 2 A chest CT scan taken at the time of diagnosis revealed rapidly progressive interstitial lung disease associated with melanoma differentiation-associated gene 5 antibody: peripheral intralobular septal thickening (arrow heads) (A) and non-septal linear or plate-like opacities (stars) (B). Peripheral and peribronchovascular consolidation (arrow) (C), perilobular opacities (stars) (D), and subpleural nonsegmental ground-glass opacities (E) were observed in the CT scan.

rapidly, which lead to significant reduction of lung volume (8). As shown in Table 1, the characteristics reported by both papers were found in our patient's chest CT taken at the time of initial diagnosis. In addition to these features of CT images of anti-MDA-5 antibody-positive ILD, the following two findings should be noted. The first was that in the early stages of the disease, opacities did not appear evenly and diffusely on both sides (11–13). This patient had significant laterality of such opacities. Second, the shadow exacerbations of some patients are slow in the early stages of the disease and then rapidly exacerbate within days (12–14). Increasing evidence highlights the striking similarities between lung injury in patients with anti-MDA-5 antibody and in those with COVID-19 pneumonia (15).

Tab. 1 Comparison of CT findings by Tanizawa et al., Chino et al., and the authors of the case report.

CT findings	Features	Researchers who pointed out the findings	Presence or absence of findings in this patient
Lower consolidation/ GGO pattern	lower peripheral or peribronchovascular nonsegmental consolidations or GGO	Takizawa et al. (Reference Number 7)	Present (Figure 2-B and C)
Lower reticulation pattern	lower peripheral or peribronchovascular reticulation	Takizawa et al. (Reference Number 7)	Present (Figure A and D)
Random GGO pattern	random peripheral GGO	Takizawa et al. (Reference Number 7)	Present (Figure C and E)
Perilobular opacities	perilobular opacities in the lower lobes	Chino et al. (Reference Number 8)	Present (Figure D)

GGO: ground-glass opacity

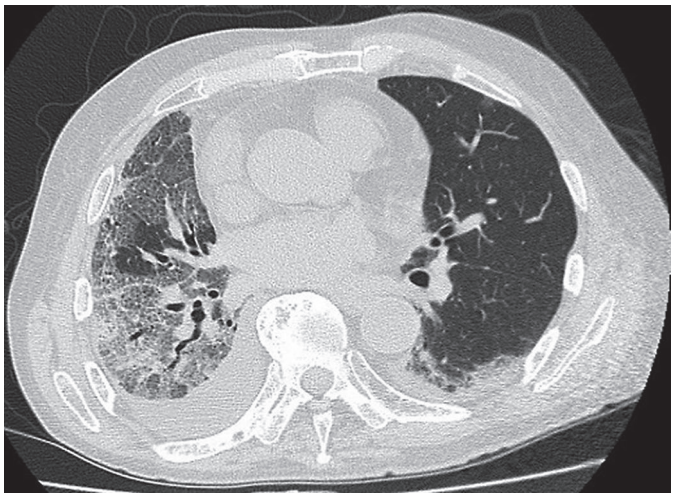

Fig. 3 A chest CT scan taken on day 9 revealed exacerbation of the ground-glass opacities in both lower lungs.

Both lung disorders can become severe and can lead to death (15). Autoantibodies against MDA5 in patients with ILD target an intracellular sensor of viral RNA (including coronavirus) that triggers the innate immune response (16). Some studies have pointed out similarities in clinical courses of these two respiratory conditions (3, 4), supported by common pathophysiological mechanisms. However, there has been no evidence that patients with COVID-19 had anti-MDA-5-antibodies. Our patient had a negative PCR for COVID-19, but the patient gradually worsened within nine days, and then rapidly deteriorated and died 14 days later. During this time, he developed a cytokine storm, similar to the course of exacerbation of COVID-19 pneumonia.

It is noteworthy that the features of anti-MDA-5-associated, rapidly progressive ILD on CT images are similar to those in patients with COVID-19 pneumonia. With regard to the 'consolidation/GGO' observed on CT scans, Zarei et al. described that consolidation and/or GGO were observed in 61% of patients, and more frequently in hospitalized patients. About another CT feature, the GGO pattern (9), Yang et al reported that GGO in patients with COVID-19 had various forms of distribution, such as peripheral, bilateral, and involved pulmonary lobes > 2 (17). Regarding 'perilobular opacities', Parry and colleagues reported that these opacities were seen late (>2 weeks) in the course of COVID-19 (10). Therefore, when such features are observed on CT images, it is necessary to consider COVID-19 infection as a differential diagnosis. Particular attention should be paid to patients who are highly positive for MDA-5 antibody.

The most characteristic feature of this patient was the prominent laterality of the opacities at the time of initial presentation. It should be considered that MDA-5 antibody-positive patients with such laterality in opacities might progress rapidly. Accumulation of information about patient background and imaging features is especially important in the treatment of rare diseases such as MDA-5 antibody-positive ILD. Chest physicians, as well as rheumatologists and dermatologists should be aware of the characteristics for optimal treatment choices.

CONFLICT OF INTEREST STATEMENT

The authors declared no conflicts of interest with respect to the authorship and/or publication of this article.

FUNDING

The authors received no financial support for the research and/or authorship of this article.

ETHICS

Written comprehensive consent was obtained from patient. Reporting of this case report was approved by the Hospital Ethics Committee.

REFERENCES

1. McPherson M, Economidou S, Liampas A, Zis P, Parperis K. Management of MDA-5 antibody positive clinically amyopathic dermatomyositis associated interstitial lung disease: A systematic review. Semin Arthritis Rheum 2022; 53: 151959.
2. Yoneyama M, Kikuchi M, Matsumoto K, et al. Shared and unique functions of the DExD/H-box helicases RIG-I, MDA5, and LGP2 in antiviral innate immunity. J Immunol 2005; 175: 2851–8.
3. Qian J, Xu H. COVID-19 Disease and Dermatomyositis: A Mini-Review. Front Immunol 2022; 12: 747116.
4. Wang G, Wang Q, Wang Y, et al. Presence of anti-MDA5 antibody and its value for the clinical assessment in patients with COVID-19: A retrospective cohort study. Front Immunol 2021; 12: 791348.
5. Kitamura M, Sugimoto H. Clinically amyopathic dermatomyositis during the COVID-19 pandemic. Oxf Med Case Reports 2021 Aug; 2021(8): omab061.
6. Giannini M, Ohana M, Nespola B, Zanframundo G, Geny B, Meyer A. Similarities between COVID-19 and anti-MDA5 syndrome: what can we learn for better care? Eur Respir J 2020; 56: 2001618.
7. Tanizawa K, Honda T, Nakashima R, et al. HRCT features of ILD in dermatomyositis with anti-CADM-140 antibody. Respir Med 2011; 105: 1380–7.
8. Chino H, Sekine A, Baba T, et al. Radiological and pathological correlation in anti-MDA5 antibody-positive interstitial lung disease: rapidly progressive perilobular opacities and diffuse alveolar damage. Intern Med 2016; 55: 2241–6.
9. Zarei F, Moezi P, Jahromi MG, Zeinali-Rafsanjani B. Comparison of chest CT findings in outpatient and hospitalized COVID-19 RT-PCR positive patients of Shiraz. J Med Imaging Radiat Sci 2022; 53: 107–12.
10. Parry AH, Wani HA, Choh NA, Shah NN, Jehangir M. Spectrum of chest CT manifestations of coronavirus disease (COVID-19): A pictorial essay. Indian J Radiol Imaging 2021; 31(Suppl 1): S170–S7.
11. Watanabe T, Takizawa N, Nagasaka T, et al. Fatal and extensive multiorgan hemorrhages in anti-melanoma differentiation-associated gene 5 antibody-positive dermatomyositis: An autopsy case report. Medicine (Baltimore) 2020; 99: e18600.
12. Kaenmuang P, Navasakulpong A. Clinical characteristics of anti-MDA5 antibody-positive interstitial lung disease. Respirol Case Rep 2020; 9: e00701.
13. Kagawa H, Tsujino K, Yamamoto Y, et al. Acute lung injury after plasma exchange in a patient with anti-MDA5 antibody-positive, rapidly progressive, interstitial lung disease: A case report. Respir Med Case Rep 2020; 29: 101016.
14. Aoyama J, Hayashi H, Yajima C, et al. Anti-MDA5 antibody-positive rapidly progressive interstitial pneumonia without cutaneous manifestations. Respir Med Case Rep 2019; 26: 193–6.
15. Mehta P, McAuley DF, Brown M, et al. COVID-19: consider cytokine storm syndromes and immunosuppression. The Lancet 2020; 395: 1033–4.
16. Dias Junior AG, Sampaio NG, Rehwinkel J. A balancing act: MDA5 in antiviral immunity and autoinflammation. Trends Microbiol 2019; 27: 75–85.
17. Yang H, Lan Y, Yao X, Lin S, Xie B. The chest CT features of coronavirus disease 2019 (COVID-19) in China: a meta-analysis of 19 retrospective studies. Virol J 2020; 17: 159.

Transient Hyperphosphatasemia in a Child with Autism Spectrum Disorder

Štěpán Kutílek[1,*], Eva Rondziková-Mlynarčíková[1], Kamila Pečenková[1], Richard Pikner[2], Tomáš Šmída[3], Eva Sládková[4], Tomáš Honzík[5], Hana Kolářová[5], Martin Magner[5]

ABSTRACT

Introduction: Autism spectrum disorder (ASD) is a neurodevelopmental disorder characterized by deficits in social communication and the presence of restricted interests and repetitive behaviors. Transient hyperphosphatasemia of infancy and early childhood (THI) is a benign laboratory disorder characterized by transiently extremely elevated activity of serum alkaline phosphatase (S-ALP).

Case Report: We present a 21-month-old girl with a right leg limp, most probably due to reactive arthritis after febrile viral infection, and deterioration of psychomotor development with concomitant transient elevation of S-ALP (61.74 µkat/L; normal 2.36–7.68 µkat/L). Normal values of serum creatinine, aspartate-aminotransferase, alanin-aminotransferase, calcium, phosphate, together with normal wrist X-ray ruled out rickets or other bone or hepatic cause of high S-ALP. The S-ALP gradually decreased within 3 months, thus fulfilling the THI criteria. Screening for inborn errors of metabolism was negative and meticulous neurologic, psychologic and psychiatric assessment pointed to the diagnosis of autism spectrum disorder (ASD). There was no causal relationship between THI and ASD, as high S-ALP was an accidental and transient finding within the routine laboratory assessment. However, when THI occurs in a child with an onset of a new disorder, or with a pre-existing bone or liver disease, it might seriously concern the physician.

Conclusion: Children with THI should be spared from extensive evaluations and unnecessary blood draws.

KEYWORDS

autism spectrum disorder; alkaline phosphatase; transient hyperphosphatasemia

AUTHOR AFFILIATIONS

[1] Department of Pediatrics, Klatovy Hospital, Klatovy, Czech Republic
[2] Department of Clinical Biochemistry, Klatovy Hospital, Klatovy, Czech Republic
[3] General Pediatric Practitioner, Klatovy, Czech Republic
[4] Department of Pediatrics, Faculty Hospital in Pilsen and Faculty of Medicine in Pilsen, Charles University, Czech Republic
[5] Department of Pediatrics and Inherited Metabolic Disorders, Faculty Hospital in Prague and 1st Faculty of Medicine in Prague, Charles University, Czech Republic
* Corresponding author: Klatovy Hospital, Klatovy, Czech Republic; e-mail: kutilek@nemkt.cz; stepan.kutilek@klatovy.nemocnicepk.cz

Received: 28 February 2022
Accepted: 28 April 2022
Published online: 29 June 2022

Acta Medica (Hradec Králové) 2022; 65(1): 41–43
https://doi.org/10.14712/18059694.2022.16

INTRODUCTION

Autism spectrum disorder (ASD) is a neurodevelopmental disorder characterized by deficits in social communication and the presence of restricted interests and repetitive behaviors (1). Prospective studies of children with ASD show that abnormalities in social communication and repetitive behaviors emerge during the second year and motor and sensory abnormalities might emerge in the first year of life (1–3). Transient hyperphosphatasemia of infancy and early childhood (THI) is a benign laboratory disorder characterized by transiently extremely elevated activity of serum alkaline phosphatase (S-ALP) in infants and toddlers without any signs of bone or liver disease. The detection of THI is mostly accidental (4–7). We present a girl with ASD and THI.

CASE REPORT

A 21-month-old girl with uneventful perinatal history and rather rapid developmental milestones (according to parents, she stood up before 8 months of age, started walking unsupported at 10 months, but had a speech delay) was intermittently feverish for one week and was also noticed with a right leg limp without any evidence of trauma, nor swelling or redness of the joints. Her parents brought her to a General Pediatric Practitioner, who ordered X-ray of the painful extremity and basic laboratory evaluation. X-ray of the right lower extremity was normal. C-reactive protein was low (<1 mg/L), thus ruling out severe ínflammation. Blood count and basic biochemical parameters were within normal pediatric age-related reference values (Table 1), with the exception of S-ALP (45 µkat/L) (Figure 1). Simultaneously, the parents noticed significant changes in the girl's behavior, such as mutism, anxiety, clumsiness, irritability, hypomimia, and no communication skills. Therefore the child was referred to a hospital, where even higher S-ALP was confirmed (Figure 1), with otherwise normal blood biochemistry, normal wrist and knees X-ray, normal abdominal ultrasound thus completely ruling out rickets and/or other bone or hepatic disease, known to be associated with high S-ALP. Both fever and limping resolved immediately upon hospital admission, and these were attributed to viral infection and, most probably, to reactive arthritis. The diagnosis of THI was established She was dismissed after three days. Furthermore, at home, the change in child's habits were more profoundly apparent and after two weeks she was hospitalized for two days with normal laboratory results, including a decline in originally high S-ALP. However, due to the change in child's behavior and a deterioration in her psychomotor development, an inborn error of metabolism was suspected. Therefore, she was then referred to a specialised center for inborn errors of metabolism. The detailed screening for inborn metabolic disorders was negative, magnetic resonance imaging of the brain was normal and a detailed psychologic and psychiatric assessment (Modified Checklist for Autism in Toddlers, Revised, M-CHAT-R, screening 9 points out of 20) was highly indicative of autism spectrum disorder (ASD). In the meantime, the S-ALP dropped to 4.15 µkat/L after 14 weeks (Figure 1). There were no other indices of bone or liver disease. Currently, the girl is five years old and is being followed-up by a specialised pediatric psychiatrist, psychologist and neurologist as the diagnosis of ASD has been confirmed.

Tab. 1 Initial basic biochemical results in our patient.

Parameter	Units	Patient	Reference value
S-ALP	µkat/L	45	2.36–7.68
S-AST	µkat/L	0.55	≤ 0.83
S-ALT	µkat/L	0.33	≤ 0.50
S-CK	µkat/L	1.67	0.4–3.82
S-creatinine	µmol/L	28	35–62
S-Ca	mmol/L	2.54	2.2–2.6
S-P	mmol/L	1.62	1.0–1.95
S-Mg	mmol/L	0.92	0.86–1.17
S-Na	mmol/L	140	134–143
S-K	mmol/L	4.4	3.3–4.6
S-Cl	mmol/L	107	96–109

Abbreviations: S-ALP – serum activity of alkaline phosphatase; S-AST – serum activity of aspartate-aminoransferase; S-ALT – serum activity of alanine-aminoransferase; S-CK – serum activity of creatinkinase; S-Ca – serum level of total calcium; S-P – serum level of phosphate; S-Mg – serum level of total magneskium; S-Na – serum level of sodium; S-K – serum level of potassium; S-Cl – serum level of chloride

DISCUSSION

THI is diagnosed incidentally in both healthy and sick children, rather a laboratory, than a clinical disorder, which is benign and self-limiting (4–7). So far, there are literature reports of THI in about 900 children, both sick and healthy. However, its incidence, based on secondary data analysis of 316 healthy infants and toddlers was estimated at 2.8% (7). The criteria for THI were first defined by Kraut et al. (8) (Table 2). THI has been also described even in adults, and in some children the S-ALP returned to normal values after more than four months (5–7). Previously

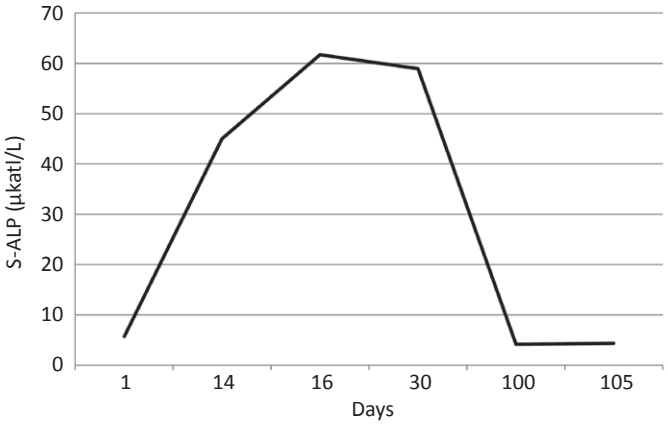

Fig. 1 Course of S-ALP in our patient. Age-related reference values 2.36–7.68 µkat/L.

Tab. 2 THI criteria devised by Kraut et al. in 1985 (8).

■ an age of less than 5 years
■ variable, unrelated symptoms
■ no bone or liver disease on physical examination or from laboratory investigations;
■ isoenzyme and isoform analysis showing elevations in both bone and liver activity
■ return to normal S-ALP values within four months

published observations ruled out either bone or hepatic disease related to THI, as parathyroid hormone levels, bone turnover markers and liver enzymes were within normal reference ranges (4–7, 9–11). THI might raise concern when encountered in children with skeletal disorders, chronic renal failure, malignancies or hepatopathy, wrongly suggesting the flare-up of the underlying disease (5, 6, 11, 12). The electrophoretic evaluation of the ALP isoenzymes and isoforms in blood samples from patients with THI revealed an atypical transient pattern of cathodal and anodal migrating fractions, similar to the isoforms of bone and liver origin (4, 5, 8, 13). THI is most probably caused by a viral infection as THI frequently occurs in children with a history of viral disease 2–3 weeks prior to the S-ALP elevation and was also observed and reported in siblings or in patients who were hospitalised together (5, 14–16). This also occurred in our patient, as febrile, most probably viral, infection preceded the detection of high S-ALP. The limping in our patient was most probably a manifestation of reactive arthritis due to a febrile viral infection. The impaired clearance of ALP from circulation is believed as the most likely cause of THI (5, 7, 11). In our patient with transiently deteriorated gait and first signs of ASD, the high value of S-ALP initially concerned the pediatrician, however the routine work-up ruled out bone or liver affection, metabolic disease, clearly pointing to the diagnosis of THI. There was no relationship between ASD and THI, as high S-ALP was an accidental and transient finding within the routine laboratory assessment. However, once THI occurs in a child with an onset of a new disorder, or with a pre-existing malignancy, bone or liver disease, it might seriously concern the pediatrician (5, 6, 11, 12, 17). Similarly, THI can alert the physician when encountered in a post-transplant patient (11, 18). It is recommended that S-Ca, P, creatinine, ALT, AST should be assessed, together with wrist X-ray to rule out rickets, renal failure or hepatopathy. Once THI is confirmed with the use of these assessments and Kraut's criteria, control S-ALP can be assessed after three months. Children with THI should be spared from extensive evaluations and unnecessary blood draws.

REFERENCES

1. Hodges H, Fealko C, Soares N. Autism spectrum disorder: definition, epidemiology, causes, and clinical evaluation. Transl Pediatr 2020; 9(Suppl 1): S55–S65.
2. Sacrey LAR, Bennett JA, Zwaigenbaum L. Early Infant Development and Intervention for Autism Spectrum Disorder. J Child Neurol 2015; 30: 1921–9.
3. Brian JA, Zwaigenbaum L, Ip A. Standards of diagnostic assessment for autism spectrum disorder. Paediatr Child Health 2019; 24: 444–60.
4. Stein P, Rosalki SB, Foo AY, Hjelm M. Transient hyperphosphatasemia of infancy and early childhood: clinical and biochemical features of 21 cases and literature review. Clin Chem 1987; 33: 313–8.
5. Kutílek S, Bayer M. Transient hyperphosphatasemia – where do we stand? Turk J Pediatr 1999; 41: 151–60.
6. Gualco G, Lava SA, Garzoni L, Simonetti GD, Bettinelli A, Milani GP, et al. Transient benign hyperphophatasemia. J Pediatr Gastroenterol Nutr 2013; 57: 167–71.
7. Huh SY, Feldman HA, Cox JE, Gordon CM. Prevalence of transient hyperphosphatasemia among healthy infants and toddlers. Pediatrics 2009; 124: 703–9.
8. Kraut JR, Metrick M, Maxwell NR, Kaplan MM. Isoenzyme studies in transient hyperphosphatasemia of infancy. Ten new cases and a review of the literature. Am J Dis Child 1985; 139: 736–40.
9. Kruse K. Normal bone turnover in isolated hyperphosphatasaemia. J Pediatr 1985; 106: 946–8.
10. Kutilek S, Cervickova B, Bebova P, Kmonickova M, Nemec V. Normal bone turnover in transient hyperphosphatasemia. J Clin Res Pediatr Endocrinol 2012; 4: 154–6.
11. Kutílek S, Skálová S, Vethamuthu J, Geier P, Feber J. Transient hyperphosphatasemia in pediatric renal transplant patients-is there a need for concern and when? Pediatr Transplant 2012; 16: E5–9.
12. Kutilek S, Stepan J, Bayer M. A case of transient hyperphosphatasaemia following vitamin D-deficient rickets. Turk J Pediatr 1993; 35: 205–7.
13. Weiber H, Fex G, Lindberg T, Skude G. Atypical, anodally migrating alkaline phosphatase isoenzyme in children and its relation to abdominal symptoms. Clin Chem 1983; 29: 593–5.
14. Kruse K, Kurz N. Further evidence for infectious origin of isolated transient hyperphosphatasaemia. Eur J Pediatr 1989; 148: 453–4.
15. Sánchez Jacob M, Escudero Gutiérrez R, Bernardo Fernández T. Transient hyperphosphatasemia in infancy. Two simultaneous cases in twins. An Esp Pediatr 1991; 35: 365–6.
16. Sakurai Y, Higashiguchi T. Transient hyperphosphatasemia: Possible association with pediatric acute respiratory infection. Pediatr Investig 2021; 5: 94–8.
17. Eymann A, Cachiarelli N, Alonso G, Llera J. Benign transient hyperphosphatasemia of infancy. A common benign scenario, a big concern for a pediatrician. J Pediatr Endocrinol Metab 2010; 23: 927–30.
18. Cole EB, Anslow M, Fadakar P, Miyashita Y, Ganoza A, Moritz ML. Transient hyperphosphatasemia following pediatric kidney transplant. Cureus 2021; 13: e17697.